Chinese Chemical Letters 36 (2025) 110423

Contents lists available at ScienceDirect

Chinese Chemical Letters

journal homepage: www.elsevier.com/locate/cclet

Antioxidative strategies of 2D MXenes in aqueous energy storage system

Li Li[a], Xue Ke[b], Shan Wang[c], Zhuo Jiang[b], Yuzheng Guo[a,b,d,*], Chunguang Kuai[b,*]

[a] The Institute of Technological Sciences, Wuhan University, Wuhan 430072, China
[b] School of Electrical Engineering and Automation, Wuhan University, Wuhan 430072, China
[c] Department of Anesthesiology, Zhongnan Hospital of Wuhan University, Wuhan 430072, China
[d] Hubei Key Laboratory of Electronic Manufacturing and Packaging Integration, Wuhan University, Wuhan 430072, China

ARTICLE INFO

Article history:
Received 1 December 2023
Revised 19 July 2024
Accepted 5 September 2024
Available online 7 September 2024

Keywords:
MXene oxidation
Mechanism
Characterization
Factors
Antioxidative strategies

ABSTRACT

As a novel two-dimensional (2D) material, MXenes are anticipated to have a significant impact on future aqueous energy storage and conversion technologies owing to their unique intrinsic laminar structure and exceptional physicochemical properties. Nevertheless, the fabrication and utilization of functional MXene-based devices face formidable challenges due to their susceptibility to oxidative degradation in aqueous solutions. This review begins with an outline of various preparation techniques for MXenes and their implications for structure and surface chemistry. Subsequently, the controversial oxidation mechanisms are discussed, followed by a summary of currently employed oxidation characterization techniques. Additionally, the factors influencing MXene oxidation are then introduced, encompassing chemical composition (types of M, X elements, layer numbers, terminations, and defects) as well as environment (atmosphere, temperature, light, potential, solution pH, free water and O_2 content). The review then shifts its focus to strategies aiming to prevent or delay MXene oxidation, thereby expanding the applicability of MXenes in complex environments. Finally, the challenges and prospects within this rapidly-growing research field are presented to promote further advancements of MXenes in aqueous storage systems.

1. Introduction

The integration of intermittent energy sources faces various challenges as the proportion of renewable sources, such as wind and solar, continues to rapidly increase in the energy market [1]. Energy storage technologies are crucial for facilitating the transition to low-carbon electricity supply, especially in harnessing intermittent energy sources [2]. In large energy storage systems, paramount importance is placed on operational safety, low installation costs, long service life, and high energy efficiency, rather than the energy density and power density that have been predominant concerns thus far [2,3]. Research interest in aqueous-based energy technologies has surged due to several merits such as: (1) Low potential risks by the utilization of non-toxic, low-volatile, and non-flammable aqueous electrolytes; (2) Simple and low-cost manufacture process that eliminates the need for oxygen-free and drying manufacturing lines; (3) high power densities guaranteed by the higher ionic mobility than organic electrolytes; (4) the absence of a solid electrolyte interphase (SEI) layer; and (5) enhanced tolerance against electrical and mechanical mishandling [4–6].

MXenes, known as two-dimensional (2D) transition-metal carbides, nitrides, and carbonitrides, have emerged as desirable candidates for aqueous energy storage applications [7,8]. MXenes are typically derived from the corresponding layered precursors called $M_{n+1}AX_n$ ($n = 1$–4) [9,10]. MAX-phase compounds have a hexagonal crystal structure consisting of $n+1$ layers of transition metals (M) interspersed with n layers of C and/or N (X), intercalated by monatomic layers of group III A or IV A elements (A) [11,12]. To obtain MXenes, the weak M-A bond is preferentially destroyed, and the A-layer is etched from the bulk precursor MAX phases [13]. During the etching process, the highly active surface atoms M react with the etching agent and solvent, producing abundant surface functional groups T_x like -F, -OH, =O, and -X [14]. The transition metal core layers ensure the metallic conductivity (>6000 S/cm), facilitating fast electron transport [15,16]. The unique layered structures of MXenes guarantee short ion diffusion distances [17]. The large redox-active surface of MXenes allows for high-rate redox (pseudocapacitive) energy storage, while the pre-intercalated water molecules contribute to excellent ion storage capacity

* Corresponding authors.
E-mail addresses: yguo@whu.edu.cn (Y. Guo), chunguangk@whu.edu.cn (C. Kuai).

https://doi.org/10.1016/j.cclet.2024.110423
1001-8417/

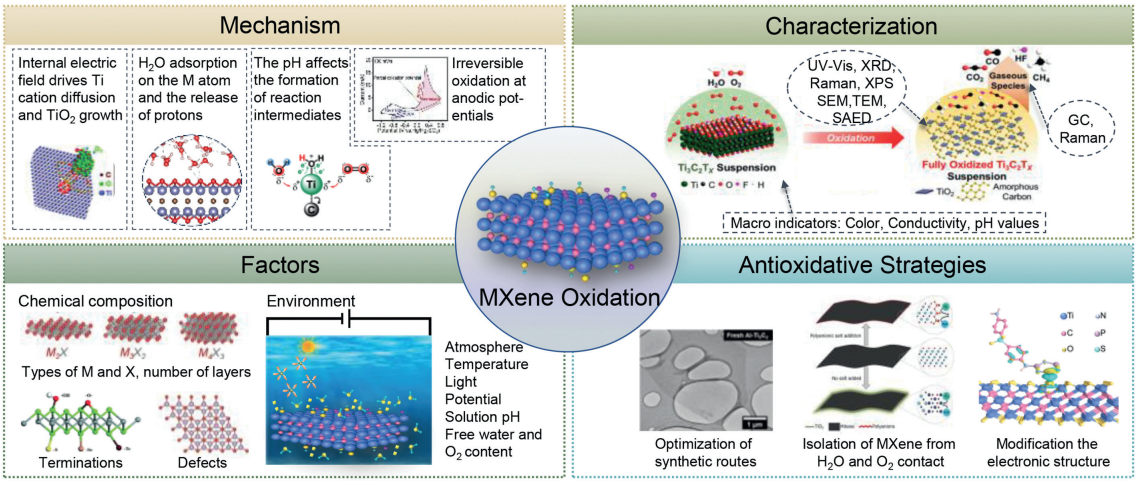

Fig. 1. Summary of oxidation mechanism of MXenes, characterization techniques, factors affecting the stability of MXenes and corresponding antioxidant strategies. Reproduced with permission [26]. Copyright 2019, the Royal Society of Chemistry. Reproduced with permission [27]. Copyright 2023, Wiley Publishers. Reproduced with permission [28]. Copyright 2021, American Chemical Society. Reproduced with permission [29]. Copyright 2019, Wiley Publishers. Reproduced with permission [30]. Copyright 2014, Wiley Publishers. Reproduced with permission [31]. Copyright 2022, the Royal Society of Chemistry. Reproduced with permission [32]. Copyright 2020, Wiley Publishers. Reproduced with permission [33]. Copyright 2021, Wiley Publishers. Reproduced with permission [34]. Copyright 2021, American Chemical Society. Reproduced with permission [35]. Copyright 2019, Wiley Publishers. Reproduced with permission [36]. Copyright 2023, Elsevier.

[18,19]. The combination of these fascinating properties makes MXenes highly promising for energy storage applications [17,20,21].

However, despite their immense potential, the synthesis, storage, device fabrication, and applications of MXenes still pose challenges. One major challenge is their susceptibility to fast structural degradation through oxidation in aqueous solutions, even under ambient conditions [22,23]. When exposed to an aqueous environment, MXene have poor chemical durability due to the structural transformation induced by collective effects of dissolved oxygen the water molecules [18,24,25]. Considering this inherent vulnerability, various efforts have been made to protect MXenes from oxidation. However, comprehensive reviews summarizing the degradation mechanism and antioxidative strategies for MXenes are relatively scarce.

We aim to present an overview of the recent progress in understanding the oxidation stability of MXenes (Fig. 1) [26–36]. We begin with a concise introduction to the synthesis methods of MXenes, followed by an exploration of their oxidation mechanisms and a summary of the currently employed methods for assessing the oxidation. Subsequently, we compile a summary of the factors that influence the stability of MXenes for guiding the design of MXene-based materials with enhanced resistance to oxidation. Additionally, recent advances focusing the antioxidant properties of MXenes are reviewed. Finally, we outline the challenges and prospects to promote further advancements in the field of MXenes. This comprehensive perspective aims to contribute to the expanding knowledge of oxidation stability in MXenes and promote their successful utilization in aqueous storage system.

2. Synthesis methods of MXenes

Considering the increasing diversity in MXenes synthesis strategies, the synthetic methods can be broadly classified into two approaches: top-down and bottom-up. The top-down approaches involve selective etching of layered bulk MAX phase to obtain MXenes, relying on the higher reactivity of the M-Al bond compared to the M-X bond in the etched environment. While the bottom-up approaches facilitate the direct formation of M-X bond products, enabling the growth of large-area 2D single crystal MXenes on the target substrate, reaching centimeter or even meter scales [37]. The synthetic parameters exert a significant influence on the shape, size, morphology, and surface chemistry of synthesized MXene, ultimately influencing the properties and performance of the MXenes [38]. This section briefly discusses various MXenes synthesis methods and their advantages/limitations used in aqueous storage system.

2.1. Top-down approaches: From bulk MAX phase to 2D MXene

Since the discovery of $Ti_3C_2T_x$ through selective etching of A atoms with hydrofluoric acid (HF) solutions in 2011 [39], HF solution has been most extensively used methods for MXenes synthesis. The MAX phases are thermodynamically stable, but the weaker metallically bonded M-A bonds are more chemically reactive compared to the M-X bonds. This reactivity allows for etching by selectively dissolving the A layers using HF. Subsequent sonication leads to the exfoliation of MXene layers with highly exposed M atoms. In an aqueous environment rich in F^-, surface reactions occur spontaneously, resulting in the formation of termination groups such as -F, -OH, and =O. Optimization of HF concentration, etching time, and temperature has been employed to obtain various MXenes (Fig. 2a) [40]. And the corresponding chemical equations are summarized in Table 1. Although this method is applicable to a wide range due to the strong binding of F^- with A elements [41], the obtained MXene nanosheets (NSs) show small lateral sizes, irregular edges, numerous pinholes and scattered dark particles [39,40]. Another challenge associated with its use is that HF is a dangerous corrosive agent, necessitating special precautions. Modified methods have been reported to prepare MXene through *in situ* HF generation, utilizing bifluoride (*e.g.*, NH_4HF_2, $NaHF_2$, and KHF_2) [42], LiF/HCl [43], NaF/HCl, KF/HCl, NH_4F/HCl [44], and FeF_3/HCl [45] as alternative sources. The optimized process allows for the delamination of MAX phases without breaking the NSs, resulting in hole-free sheets with well-defined and clean edges (Fig. 2b). Moreover, multilayer MXene NSs can be easily converted to monolayer NSs through milder manual shaking facilitated by the intercalation of solvated Li^+, obtaining NSs with transverse dimensions up to micron level. Moreover, MXenes exhibit excellent hydrophilicity due to the presence of surface O-containing groups and a high negative surface charge, enabling easy dispersion in water and solution processing capabilities [41].

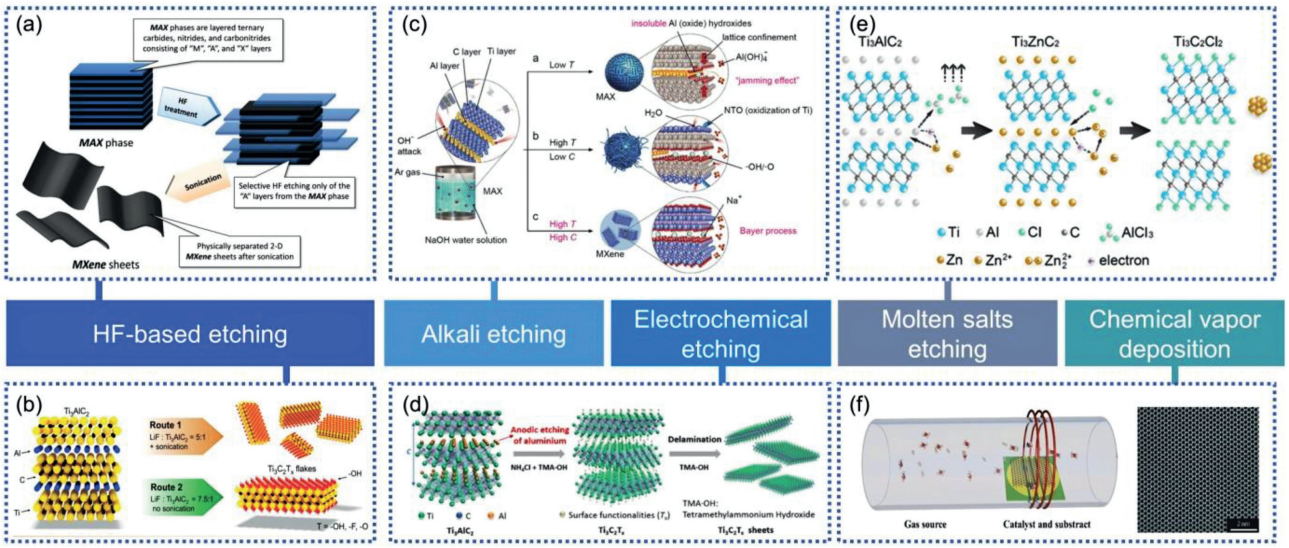

Fig. 2. MXene synthesizing techniques. (a, b) HF-based etching. Reproduced with permission [40]. Copyright 2012, American Chemical Society. Reproduced with permission [97]. Copyright 2016, Wiley Publishers. (c) Alkali etching. Reproduced with permission [48]. Copyright 2018, Wiley Publishers. (d) Electrochemical etching. Reproduced with permission [52]. Copyright 2018, Wiley Publishers. (e) Molten salts etching. Reproduced with permission [54]. Copyright 2019, American Chemical Society. (f) Chemical vapor deposition. Reproduced with permission [37]. Copyright 2022, Wiley Publishers.

Table 1
The representative synthesis methods for MXenes.

Synthesis method	Chemical equation	Ref.
HF-based etching	$M_{n+1}AlX_n + 3HF = M_{n+1}X_n + AlF_3 + 1.5H_2$ $M_{n+1}X_n + 2H_2O = M_{n+1}X_n(OH)_2 + H_2$ $M_{n+1}X_n + 2HF = M_{n+1}X_nF_2 + H_2$	[40]
Alkali etching	$Ti_3AlC_2 + OH^- + 5H_2O = Ti_3C_2(OH)_2 + Al(OH)_4^- + 2.5H_2$ $Ti_3AlC_2 + OH^- + 5H_2O = Ti_3C_2O_2 + Al(OH)_4^- + 3.5H_2$	[48]
Electrochemical etching	$Ti_3AlC_2 - 3e^- + 3Cl^- = Ti_3C_2 + AlCl_3$ $Ti_3C_2 + 2OH^- - 2e^- = Ti_3C_2(OH)_2$ $Ti_3C_2 + 2H_2O = Ti_3C_2(OH)_2 + H_2$	[52]
Molten salts etching	$Ti_3AlC_2 + 1.5ZnCl_2 = Ti_3ZnC_2 + 0.5Zn + AlCl_3$ $Ti_3ZnC_2 + ZnCl_2 = Ti_3C_2Cl_2 + 2Zn$	[54]

Alkali-etching strategy, a HF-free methode with gentler reaction conditions, has been recognized as a potential environmentally friendly method for MXene preparation. From a thermodynamic perspective, A atoms like Al can react with OH^- under standard thermodynamic state. Xie *et al.* developed a preparation procedure that involves the surface treatment of bulk Ti_3AlC_2 in an aqueous NaOH solution, followed by a H_2SO_4 hydrothermal treatment. The etching of the Al atoms mostly occurs only on the outer surface of the bulk MAX phase, obtaining Ti_3C_2 layers with -OH groups [46]. This strategy verifies that alkali-etching is effective for MAX etching; however, only the superficial layer of the MAX phase can be etched, leading to an exceedingly low MXene yield. The separation of etched MXenes from their MAX phase precursors presents challenges. Oxide/hydroxide layers may still be present alongside MXene during alkali exposure, hindering the production of pure MXenes [47]. Li *et al.* reported a NaOH-assisted hydrothermal method (using 27.5 mol/L NaOH, 270 °C) to etch Ti_3AlC_2 to prepare $Ti_3C_2T_x$ (T = OH, O) with 92 wt% purity (Fig. 2c) [48]. The mechanism involves the oxidation of Al into Al (oxide) hydroxides, followed by the dissolution of these compounds in alkali. Etching the MAX phase with concentrated bases proves effective, yielding highly hydrophilic F-free terminated MXenes. However, the use of high concentrations of alkali and high temperatures poses safety concerns and limits its applicability for large-scale MXene production. In addition, the products obtained typically consist of multilayered MXene with an accordion-like morphology, necessitating further embedding and delamination processes to obtain monolayered MXene NSs.

In essence, the selective etching mechanism is an electrochemical process that involves the transfer of charge from the etched material to other compounds. The Al layers, being in a more oxidized state than M, are more easily extracted. The electrochemical etching route has shown promising effectiveness in selectively extracting nanolaminate materials from MAX precursors by adjusting the etching parameters [49]. To selectively remove the A layers while preserving the 2D structure of MXene, the modulation of electrolytes, applying voltage, and etching time are crucial. Anodic etching of MAX in dilute HF, HCl, and NaCl solutions, for example, leads to excessive etching of both M and A layers, yielding amorphous carbide-derived carbons (CDCs) [50]. The first successful synthesis of Ti_2CT_x with -Cl, -O and -OH terminations *via* electrochemical etching in HCl electrolyte was reported. Gradually increasing the voltage further removes M layers, producing CDCs, with the CDC layers on the surface inhibiting further etching [51]. While the electrochemical methode offers advantages such as low reaction temperature and minimal corrosive acid usage, the yield of MXene nanosheets is insufficient for practical applications due to the concomitant presence of CDC layers impeding further etching. Yang *et al.* proposed an effective strategy based on the anodic corrosion in a binary aqueous electrolyte (1.0 mol/L NH_4Cl and 0.2 mol/L TMA·OH) to enhance the inner accessibility of the MAX phase. This process involves preferential removal of Al followed by

in situ intercalation of TMA^+, leading to the formation of MXene flakes ($Ti_3C_2T_x$, T = O, OH) with large average dimensions (18.6 μm) and high yields (above 90%) (Fig. 2d) [52]. Nonetheless, the toxicity of the intercalants raises concerns regarding laboratory safety and health. Pang *et al*. carried out a thermal-assisted electrochemical etching route to generate flower-like MXene up to 25 μm. Mild heating, in the presence of dilute hydrochloric acid etching solution, will accelerates the kinetics of the etching process. MXene NSs prepared through electrochemical etching possess enriched -O/OH terminations, large lateral size and high electrical conductivity, which are very attractive in multi-functional electrocatalysis and energy storage applications. However, two obstacles remain for large-scale preparation: insufficient yield due to the presence of CDCs layers and the low generalizability limited to Al-based MAX.

Surface functional groups are the key factor affecting the properties of MXenes, molten salt etching is an effective method for synthesizing MXenes with various termination groups. In this method, molten fluoride salts (LiF, NaF, and KF) [53], Lewis acidic molten salts (NaCl, KCl, $CdCl_2$, $FeCl_2$, $CoCl_2$, $CuCl_2$, AgCl, $NiCl_2$, CuI, $CuBr_2$, *etc*.) [54,55] are used to selectively etch A layers from MAX precursor at high temperatures. The etching mechanism primarily relies on the substitution reaction between metal cations in Lewis acidic molten salts and zero-valence A-site atoms in MAX precursors. The choice of molten salts enables the regulation of MXene functional groups. Huang and colleagues synthesized exclusively Cl-terminated MXenes in $ZnCl_2$ molten salts for the first time (Fig. 2e) [54], and subsequently achieved I- and Br-terminated MXenes by employing CuI and $CuBr_2$ molten salts as Lewis acidic etchants [55]. The Cl-terminated MXenes demonstrated increased lattice symmetry, improved stability, and superior electrochemical performance compared to F-terminated ones [56,57]. This discovery has inspired the design of functional terminations for MXenes. On this basis, MXenes with Ti-Br and Ti-Cl bonds, which have low bond dissociation energies, can undergo chemical modification through exchange reactions with desired atoms and functional groups [58]. Kamysbayev *et al*. proved that etching MAX phases in molten $CdBr_2$ yields Br-terminated MXenes, which can further undergo substitution with -O, -S, -Se, -Te, and -NH groups, or form vacancy sites. These surface terminations can influence physicochemical properties. For instance, Nb_2C MXenes exhibit superconductivity dependent on surface groups [59]. Compared to HF based etching protocol, this strategy can avoid producing highly toxic liquid waste, regulate surface terminations, and broaden the synthesis of non-Al MAX precursors based MXene (A = Si, Zn and Ga). The aqueous etching method is applicable to the majority of aluminum-containing MAX phases at low working temperatures, yielding hydrophilic MXenes. However, this aqueous system proves ineffective for non-Al MAX or nitrogen-containing MAX phases. The theoretical calculation has shown that the cohesive forces within $Ti_{n+1}N_n$ MXenes are lower than those in $Ti_{n+1}C_n$ MXene, while the formation energy (ΔE_f) of $Ti_{n+1}AlN_n$ surpasses that of $Ti_{n+1}AlC_n$. Consequently, the Al within the nitride MAX phase exhibits stronger bonding compared to its carbide counterparts, rendering extraction more challenging [60]. Second, nitride MXenes exhibit suboptimal thermal stability under corrosive conditions [9,11]. Thus, for MXenes with elevated nitrogen content, it is advisable to employ less aggressive Lewis acids, or alternatively, the chemical vapor deposition (CVD) method, to refine synthesis conditions for subsequent experimental endeavors. Moreover, due to the negative effects of -F on electrochemical properties and material stability in aqueous solution systems, fluorine-free etching methods is developing rapidly. However, in contrast to HF-MXene, the Cl-and O-terminated MXenes show poor electrochemical signature in the aqueous electrolyte due to the its relatively hydrophobic surface [55,61]. Moreover, the etching and surface group substitution/elimination reactions in molten inorganic salts are all performed in Ar-filled glovebox, which increases the experiment cost and threshold [54,59].

2.2. Bottom-up approaches: From atoms to 2D MXene

Direct bottom-up approaches would directly generate the M-X bond products without the need for intermediate MAX phases, facilitating practical applications of MXene-based materials. Among these approaches, CVD demonstrates remarkable competitiveness in terms of controllability, uniformity, and scalability [37]. The growth of MXene crystals *via* CVD involves the reaction of carbon or nitrogen sources with transition metal atoms on a smooth and uniform liquid metal surface at high temperatures (Fig. 2f). Precise control over the size, morphology, thickness, and crystallinity of MXene crystals can be achieved by adjusting growth parameters such as temperature, growth time, pressure, flow rate, and catalysts. The first report by Xu *et al*. described the fabrication of defect-free and impurity-free 2D ultrathin α-Mo_2C crystals through CVD, utilizing methane as the carbon source and a Cu foil on a Mo foil as the catalyst at temperatures above 1085 °C [62]. The obtained α-Mo_2C crystals had nanometer-scale thickness, lateral sizes exceeding 100 μm, and high stability in air for several months. During the CVD synthesis of MXene, gaseous reagents react with the catalyst surface. As the growing MXene carpet becomes thicker, the diffusion of gaseous reagents towards the reaction zone slows down, leading to a self-limiting growth of the MXene carpet. Wang *et al*. observed a new growth regime that overcame this kinetic bottleneck [63]. This synthesis involved the high-temperature reaction between metals, metal halides, and graphite, methane, or nitrogen. It generated MXene carpets and complex spherical morphologies by CVD, which were formed by bending and releasing of the MXene carpets, exposing new surfaces for further reactions. Directly synthesized MXene has a vertically aligned carpet-like structure, showing easily accessible surfaces and exposed catalytically active edges. Under certain growth conditions, the sheets could detach from the surface to form vesicles, enabling large-scale preparation. This process also avoids the degradation in quality that may occur during the transfer stage from the substrate. Although only a few years have passed since the initial growth of MXene crystals by CVD, there is ample room for improvement. For example, the CVD process involves numerous influencing factors, necessitating further studies on the growth mechanism of CVD-prepared MXenes. Additionally, it is imperative to consider other bottom-up synthesis methodologies, including template-assisted synthesis and plasma-enhanced pulsed laser deposition (PELPD) methods [16,21]. Xiao *et al*. introduced a scalable approach leveraging the reduction of 2D hexagonal oxides in a NH_3 atmosphere to yield 2D nitrides like MoN, W_2N, and V_2N [16]. Notably, the salt-templated technique exhibits high yield and efficiency due to its easily scalable synthesis, achieved by modulating salt quantities, and the recyclability of the salt for subsequent use. Moreover, the resultant 2D MoN nanosheets demonstrate excellent dispersibility in deionized water, with negatively charged surfaces facilitating cation intercalation, thus offering promising prospects for printable and flexible electronic applications. Ultrafine Mo_2C films were also fabricated *via* PELPD [21], employing methane plasma as the carbon source and Mo vapor generated through pulsed laser ablation. The reaction took place on a sapphire substrate heated to 700 °C, yielding high-quality films with adjustable thickness controlled by varying the laser pulse rate.

3. Oxidation mechanism of MXenes

In MXenes, the X atoms occupy the octahedral interstitial sites of the M atoms in the hexagonal crystal sublattice, creating a tightly packed structure. The large number of exposed M atoms on

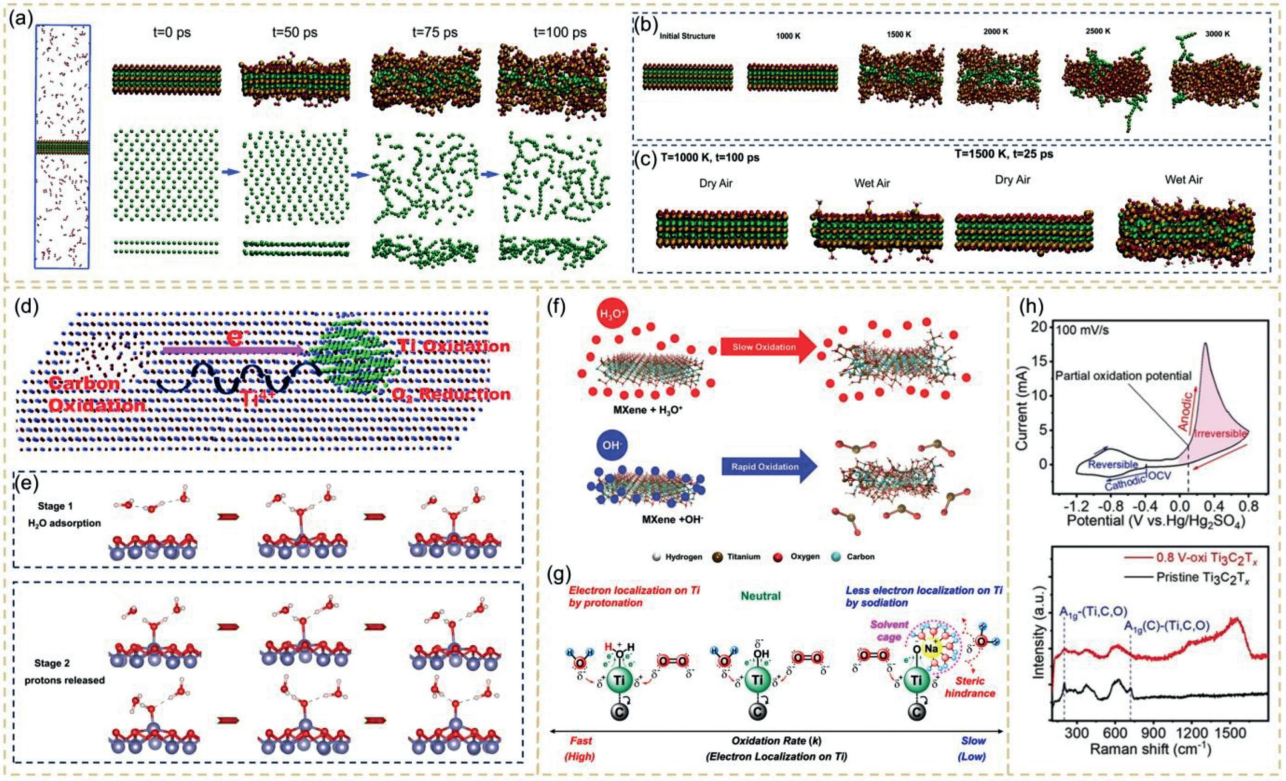

Fig. 3. The Oxidation Mechanism of MXenes. (a) Changes in configuration of the MXene structure after 0, 50, 75, and 100 ps oxidation in an oxygen atmosphere at 1500 K (Ti: tan, C: green, and O: red). (b) MXene structure after oxidation in oxygen at different temperatures. (c) Comparison of MXene oxidation in oxygen and oxygen/water environments. Reproduced with permission [68]. Copyright 2018, the Royal Society of Chemistry. (d) Illustration of internal electric field formation in Ti_3C_2 oxidation. Reproduced with permission [26]. Copyright 2019, the Royal Society of Chemistry. (e) The oxidation process in V_2CO_2-H_2O systems. Reproduced with permission [27]. Copyright 2023, Wiley Publishers. (f, g) Schematic for MXene oxidation in aqueous dispersions with acidic and alkaline pH. Reproduced with permission [28]. Copyright 2021, American Chemical Society. Reproduced with permission [71]. Copyright 2020, Wiley Publishers. (h) Irreversible electrochemical behavior of $Ti_3C_2T_x$ at anodic potentials. Reproduced with permission [33]. Copyright 2021, Wiley Publishers.

the surface makes MXenes thermodynamically substable and susceptible to reactions with oxidizing agents [64,65]. Therefore, after the weaker M-A bonds are broken during the etching process, the undercoordinated M-metal surface reacts with the T_x substance in the etchant and saturates rapidly again [66,67]. When MXene was heated in vacuum, the structure of MXene did not change significantly. Only at temperatures above 1500 K, the Ti and C atoms rearrange to form a cubic TiC structure. Therefore, in the environment without oxidizer, the structure of MXene is stable at low temperature and still undergoes a topological transition at high temperature. The oxidation of the MXene structure in oxygen and water atmosphere was investigated by ReaxFF-based molecular dynamics simulations. In O_2 atmosphere at 1500 K (Fig. 3a), there are no significant structural changes in MXene within 25 ps of simulation time. However, after 50 ps, some Ti atoms on the MXene surface form bonds with O_2 molecules. Over time (75 and 100 ps), Ti atoms from the middle layer diffuse to the surface and react with O_2 molecules, resulting in a completely distorted structure. This will cause the two separated C layers to come closer, resulting in the formation of C–C bonds. After 75 ps, C atoms bond with each other, resulting in a carbon substrate. Moreover, the oxidation of MXene is temperature dependent (Fig. 3b). At 1000 K, no surface functionalization or formation of TiO_2 nanoparticles occurs. At 1500 K and 2000 K, C atoms bind to form a C substrate. At higher temperatures, surface openings appeared in the top and bottom layers of MXene, and defects enlarge over time as C atoms migrate towards the surface. At 2500 K, carbon chains diffuse to the surface, and at 3000 K, some carbon chains are released into the gas phase. At 100 ps and 1000 K, the MXene structure was stable in an oxygen atmosphere (Fig. 3c), but Ti atoms migrate to the surface and functionalize it with O and OH groups in a H_2O/O_2 atmosphere. Similar phenomenon was observed at 25 ps and 1500 K. The oxidation rate of MXene is faster in the presence of H_2O molecules [68]. In actual working conditions, especially in solution environments, such high ambient temperatures will not be reached, but due to MXene's defects and the influence of the external environment, oxidation phenomena can occur even at room temperature.

Xia *et al.* investigated the oxidation mechanism of MXene flakes at atomic level using aberration-corrected scanning transmission electron microscopy (STEM) [26]. The electrons flowing out of the faulty region is accompanied by the presence of Ti-vacancies, which creates an internal electric field and initiates the formation of carbon clusters (Fig. 3d). Regions with Ti vacancies exhibit positive charge, and the C^{4-} is susceptible to loss electrons and is oxidized, which promotes the nucleation of C^0-cluster and amorphous carbon aggregations. As carbon undergoes oxidation, electron holes accumulate, resulting in excessive positive charge in these regions. The excess electrons tend to accumulate to form a negatively charged region at concave locations such as wrinkles, atomic steps, and corrugated surfaces, thus creating an instantaneously internal electric field. In the presence of this internal electric field, Ti cations diffuse toward the negative pole, which react with electron-acquiring O^{2-} to form anatase TiO_2, allowing more C to be oxidized at the positive pole. And the generated anatase TiO_2 crystals with the {101} crystallographic plane is perpendicular to the {0001} basal plane of $Ti_3C_2T_x$. Furthermore, various factors influence the oxidation of MXenes at room temperature, including exposure to O_2 and structural defects in the synthesized MXenes.

While the formation of metal oxides from M elements is generally accepted, the form in which carbon is present remains controversial. Some reports assumed that carbon and nitrogen eventually produce gaseous substances during oxidative transformations in aqueous environments, which may be CH_4, CO, CO_2, N_2, *etc.* Transformation products of different MXenes were studied using gas chromatography (GC), Raman spectroscopy, and solution pH measurements. Carbide MXenes transform into metal oxides and CH_4, while carbonitride MXenes transform into metal oxides, CH_4, and NH_3 [24]. The formation of these end products is thought to involve multiple stages, but the specific mechanisms behind their formation remain unclear.

Zhang *et al*. explored the degradation behavior of $Ti_3C_2T_x$ MXene colloidal solutions under different environments using scanning electron microscopy (SEM), transmission electron microscopy (TEM), Ultraviolet-visible (UV–vis), Raman spectroscopy, and X-ray photoelectron spectroscopy (XPS) [69] Oxygen with high solubility in water supplies a sequential oxidant source for MXene degradation, whereas in hermetic Ar-filled environment, water slowly degrades MXene flakes without the dissolved oxygen. The role of water in degradation processes involving MXene NSs is still considered mainly solvent-related, with dissolved oxygen acting as the primary oxidizing agent. Huang *et al*. established the role of water in oxidation by comparing the stability of $Ti_3C_2T_x$ and Ti_2CT_x in aqueous and nonaqueous colloids exposed to O_2 or Ar environments [70]. Oxidation kinetics was monitored using UV–vis transmittance and Raman spectroscopy. The time constant of $Ti_3C_2T_x$-isopropanol/O_2 is ~2026 days while the time constant of $Ti_3C_2T_x$-water/Ar is ~41 days. In the degradation processes of MXenes, particularly in $Ti_3C_2T_x$ and Ti_2CT_x systems, water, rather than O_2, plays a primary role.

Hou *et al*. developed a neural network potential (NNP) for aqueous MXene systems, which combines combining deep neural networks and active learning scheme. This novel approach allowed for the systematic investigation of the oxidation behavior of ultralarge aqueous V_2CO_2-H_2O systems (Fig. 3e) [27]. The entire oxidation process can be approximately divided into two periods: the adsorption of water molecules on V atoms and the subsequent release of protons. Firstly, the O atoms in the H_2O are directed towards the V_2CO_2 surface, causing the V atom to shift from its original position and form a V-O bond. Secondly, due to the interaction with the two nearest H_2O, the two O–H bonds of adsorbed H_2O break one by one as the length of the V-O bond decreases, resulting in the formation of stable vanadium oxide on the surface. Importantly, the presence of free protons and oxides significantly inhibits subsequent oxidation reactions, resulting in an exponential decay of the oxidation degree over time. This behavior is consistent with experimentally measured oxidation rates. In addition, the developed NNP, with the addition of new data, can be used for other applications in complex MXene aqueous systems. This breakthrough paves the way for the future development of effective protection strategies to control and preserve the stability of MXenes.

Although many studies have been reported on the role of dissolved O_2 and H_2O in the oxidation process, the underlying mechanisms of MXenes in aqueous environments are unknown and need to be further explored. In aqueous energy storage systems, there is a wide range of electrolytes, of which pH is also considered to be a key factor affecting the oxidation of MXene. It is worthwhile to explore the oxidation mechanism of MXene under different pH conditions. Zhao *et al*. investigated the oxidation kinetics of $Ti_3C_2T_x$ in dispersions with initial pH range from 2 to 10 to elucidate the oxidation mechanism of MXene in aqueous solution (Fig. 3f) [71]. In alkaline solutions, higher atomic percentage of Ti(IV) component and faster declines of electrical conductivity indicate an accelerated oxidation process. On the one hand, OH^- ions in solution react with the protons dissociated from the -OH groups on MXene flakes surface to generate unstable -O^-, which is more active to undergo oxidation reactions. On the other hand, OH^- ions may be adsorbed and react with the positively charged MXene edges, leading to chemical degradation. The active MXene edges may first react with OH^- and H_2O, so the oxidation rate of MXene sheets is slower in acidic conditions. In addition, the strong acids may lead to the formation of defects that create more reaction sites, also leading to a faster oxidation rate. After integrated analysis, Doo *et al*. found that the oxidation products of MXene are solid products (*e.g*., TiO_2 and amorphous carbon) and a variety of gaseous substances, including CH_4, CO, CO_2, and HF [28]. The generated CO_2 and HF gases dissolved in water are responsible for the decrease of the pH in oxidation of aqueous-phase $Ti_3C_2T_x$ suspensions. The kinetics of the oxidation process was studied by UV–vis absorbance spectra. It was found that the acidic pH of the aqueous $Ti_3C_2T_x$ colloid was favorable for the oxidation reaction and the basic pH was inimical to the oxidation reaction (Fig. 3g). The oxidation reaction is a nucleophilic addition reaction starting from the surface -OH, and the H^+ and OH^- ions influence the oxidation reaction by coordinating with -OH. Under acidic conditions, the -OH is protonated by H^+ ions, resulting in enhanced electron localization on O atoms in the Ti-O bond, and the electron-deficient Ti atoms are more sensitive to O atoms from H_2O and/or O_2. Vice versa, in alkaline conditions, the -OH deprotonates and coordinates with alkali metal ions forming a stable intermediate (Ti-O-Na^+) that can trap water to form a huge solvent cage. The less electrophilicity of the intermediate and the steric effect of the solvent cage would suppress the attack of the oxidizing agent.

The electrochemical stability of MXene is a significant but neglected issue for energy storage systems. In general, MXene is more suitable as an anode (cathode) material due to its relatively negative electrochemical potential window. MXene operates at cathodic potentials (−1.2 V to −0.2 V *vs.* Hg/Hg_2SO_4) and exhibits a pair of redox peaks in acidic electrolytes (Fig. 3h) [29]. However, $Ti_3C_2T_x$ is susceptible to irreversible oxidation at anodic potentials higher than 0 V *vs.* Hg/Hg_2SO_4. The anodically oxidized MXene lattice expands and the surface composition changes, forming amorphous carbon (TiO_2 dissolves in acidic electrolyte). By analyzing the components and structure of anodized MXene, a decrease in the Ti and F content of the samples was found. Lorencova *et al*. hypothesized that the outer layer of $Ti_3C_2T_x$ containing F groups undergoes an oxidation reaction at anodic potential $Ti_3C_2F_x + 8H_2O \rightarrow 3TiO_2 + 2CO + 16H^+ + (16\text{-}x)e^- + xF^-$, forming a TiO_2 layer or a TiO_2 structural domain [72]. In presence of F^- ions, TiO_2 is subsequently dissolved by forming a complex with fluoride ions $TiO_2 + 4H^+ + 6F^- \rightarrow [TiF_6]^{2-} + 2H_2O$.

4. Detecting the oxidation of MXenes

In the aqueous environment, along with the inevitable oxidation reaction of MXene, the structure and chemical composition will change, which will adversely affect its excellent performance. It is vital to assess MXenes structure, surface chemistry and composition of MXenes *via* reliable characterization techniques. Visual assessment is the initial step in characterizing MXene oxidation, and its significance is often overlooked. Each MXene exhibits unique colors associated with its optical properties, reflecting its structure and composition [73]. For example, Ti-based MXenes ($Ti_3C_2T_x$ or Ti_2CT_x) will appear "milky" or white when oxidized, indicating the formation of TiO_2 [74]. In the case of V-based MXenes, the visible sign of oxidative degradation is the change in color of the supernatant which is due to the dissolved vanadium oxide species [75]. While color change provides a convenient primary observation, it is prone to variability. Therefore, the degree of MXene oxidation should be accurately determined using diverse spectroscopy and electron microscopy techniques. It is well known

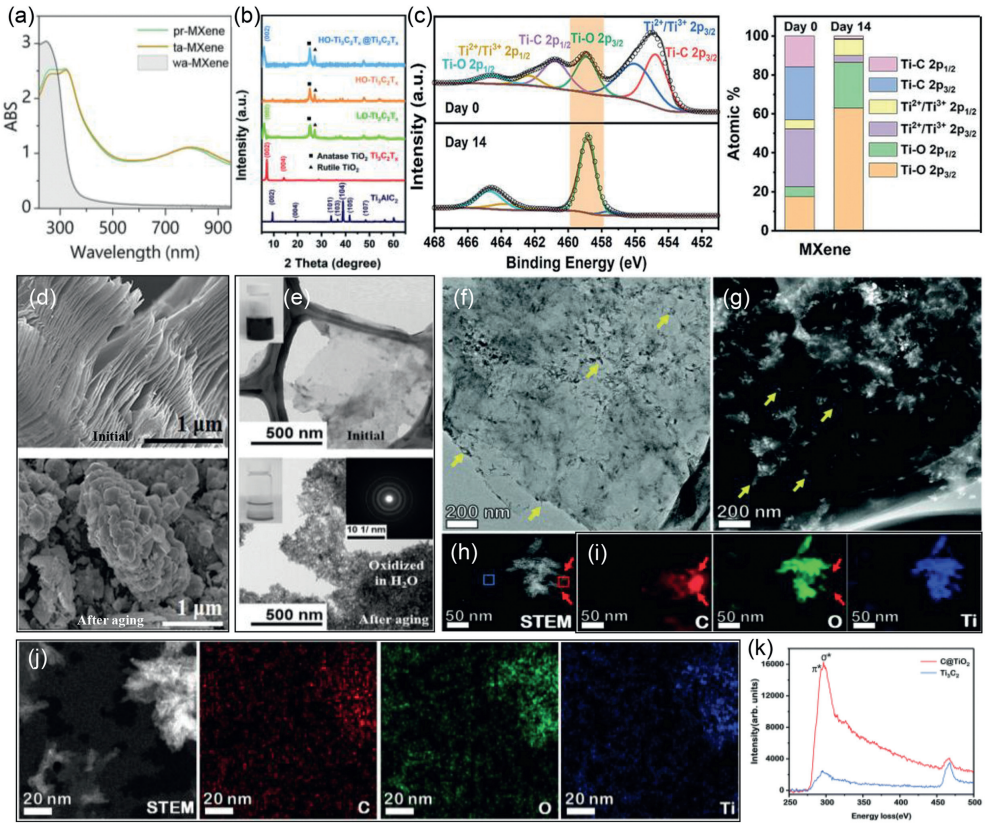

Fig. 4. (a) UV–vis spectra for MXene dispersion (pr-MXene) and the aged dispersions (wa-MXene). Reproduced with permission [76]. Copyright 2021, Elsevier. (b) XRD patterns of Ti_3AlC_2, $Ti_3C_2T_x$, lightly oxidized $Ti_3C_2T_x$ (LO-$Ti_3C_2T_x$), heavily oxidized $Ti_3C_2T_x$ (HO-$Ti_3C_2T_x$), and HO-$Ti_3C_2T_x$@$Ti_3C_2T_x$. Reproduced with permission [77]. Copyright 2021, the Royal Society of Chemistry. (c) High-resolution Ti 2p XPS spectra of MXene and corresponding XPS peak fitting results. Reproduced with permission [79]. Copyright 2022, Wiley Publishers. (d) SEM and (e) TEM images of initial $Ti_3C_2T_x$ (top) and after aging for 28 weeks (bottom). Reproduced with permission [74]. Copyright 2021, Wiley Publishers. (f) Bright-field TEM and (g) dark-field STEM images of $Ti_3C_2T_x$ flakes. (h) HAADF-STEM image and (i) EDS elemental maps. (j) HAADF-STEM image and corresponding EDS maps. (k) EELS spectra for the red box (amorphous carbon) and blue box ($Ti_3C_2T_x$ substrate). Reproduced with permission [26]. Copyright 2019, the Royal Society of Chemistry.

that the oxidation products of MXene are not only solid products like TiO_2 and amorphous carbon but also various gaseous substances such as CH_4, CO, and CO_2. The degree of MXene oxidation can be detected by measuring the emergence of solid products *via* UV–vis, X-ray diffraction (XRD), XPS, SEM, and TEM coupled selected area electron diffraction (SAED), aberration-corrected STEM, X-ray energy dispersive spectroscopy (EDS) coupled with electron energy loss spectroscopy (EELS).

UV–vis spectroscopy is a fast and cost-effective method to quantitatively monitor MXenes colloidal oxidation degree [33]. As illustrated in Fig. 4a, the strong absorbance in region of 200–400 nm and 700–850 nm can be attributed to the $Ti_3C_2T_x$ MXene in solution. And the transmittance at 237 nm is ascribed to TiO_2, and the intensity of the peak increases as oxidation proceeds. The intensity of normalized peak at ≈785 nm, which is attributed to the valence state of Ti in the $Ti_3C_2T_x$ [76], allows real-time monitoring of MXene concentration and lifetime prediction. This method can also be applied to evaluate the influence of environmental factors such as solvent, concentration, and pH on the oxidation kinetics of MXene, and provide strategies for improving the antioxidant properties of MXene. XRD is a commonly used technique for determining both the crystal structure and *d*-spacing of fresh and oxidized MXene [41]. As the degree of oxidation increases, the intensities of the typical peaks of MXene decrease proportionally, while new peaks at around 25.3° and 27.2° for anatase and rutile TiO_2 increase. The (002) peak at around 7° is downshifted to around 6°, with an expanded interlayer distance, which is caused by the lattice expansion by formation TiO_2 nanoparticles in irreversible oxidation process [29]. HO-$Ti_3C_2T_x$ exhibited the disappearance of the (002) peak, indicating the destruction of the laminar structure, while the peaks corresponding to anatase and rutile TiO_2 remained (Fig. 4b) [77]. However, the initially formed oxide is typically amorphous and cannot be detected by XRD.

Raman spectroscopy, which measures phonons or lattice vibrations, can provide valuable insights into the chemistry changes and bonding that occur during the oxidation process, thereby offering important information about the MXene structure. This technique is capable of detecting molecular fingerprints and is sensitive to traces of amorphous compounds and transition metal oxides that are commonly present during oxidation [78]. Comparing the Raman spectra of pristine $Ti_3C_2T_x$ and oxidized $Ti_3C_2T_x$, a reduction in the relative intensities or even disappearance of the MXene peaks at 205 and 723 cm^{-1} was observed. These peaks correspond to the out-of-plane vibrations of Ti, C, O atoms, and C atoms in $Ti_3C_2T_x$, respectively (Fig. 3e). The decrease in intensity of these peaks may be attributed to the effect of nearby defects and cavities, which weaken the out-of-plane vibrations. An observable broad peak around 1580 cm^{-1} in oxidized $Ti_3C_2T_x$ may be related to the presence of C–C bonds in amorphous carbon formed during the oxidation process [29]. It is imperative to recognize that excessive laser power, sufficient to induce sample oxidation, can result in MXene NSs degradation. During the test procedure, meticulous attention must be given to the judicious selection of laser power, magnification, and laser wavelength to ensure accurate and reliable results. XPS analysis is capable of providing valuable information regarding the chemical and bonding changes during $Ti_3C_2T_x$

oxidation. By analyzing the deconvoluted Ti 2p spectra of $Ti_3C_2T_x$ (Fig. 4c), multiple components represent various oxidation states, such as Ti-C 2p, Ti^{2+}/Ti^{3+} 2p, and Ti-O. The proportion change of Ti-O $2p_{3/2}$ (458.9 eV) peak proves the growth of TiO_2 on the lamellar surface. The percentage of Ti-O $2p_{3/2}$ of MXene increased from 17.5% to 63% after 14 days under ambient conditions [79].

SEM and TEM allow visualization of the structure and allows direct observation of the formation of TiO_2 NPs during the oxidation process. After aging for 28 weeks, the $Ti_3C_2T_x$ samples showed visible oxide particles in the interlayers, which was considered to be concrete evidence of oxidation, leading to the destruction of laminated structure (Figs. 4d and e). In addition, SAED pattern in the inset confirms that $Ti_3C_2T_x$ has transformed into amorphous TiO_2, as it does not have a symmetric hexagonal structure [74]. STEM, EDS coupled with EELS are effective means of investigating the structural changes during MXene oxidation at the atomic level. Bright-field TEM images with enhanced diffraction contrast has sharper contrast of the MXene substrate, while high-angle annular dark-field (HAADF)-STEM images display greater thickness and atomic number contrast, enabling convenient observation of TiO_2 nanocrystals. The nanoparticles are observed at the edge and on top of the MXene flakes, as indicated by the yellow arrows (Figs. 4f and g). Elemental mappings using EELS (Fig. 4i) and EDS (Fig. 4j) affirm that the bright nanoparticles predominantly consisted of Ti and O. The bright nanoparticles (TiO_2) are more visible than the flakes due to the oxidation process where Ti atoms diffuse from the flakes to form nanoparticles with higher thickness. Carbon aggregates have been observed in the EELS elemental diagram (Fig. 4i), as indicated by the red arrows. Comparing the EELS spectra (Fig. 4k) of the oxidized region and the MXene substrate (Fig. 4h), the spectrum of the oxidized region has a strong C–C π^* edge at 280 eV, whereas the C edge collected from MXene has no significant π^* edge, certifying the amorphous nature of the carbon. Therefore, the oxidation products of $Ti_3C_2T_x$ MXene are TiO_2 nanoparticles and amorphous carbon $Ti_3C_2 + 3O_2 = 3TiO_2 + 2C$.

Additionally, the use of gas analysis provides a powerful technique for better understanding the conversion mechanism of MXene. Huang *et al.* used GC to investigate the gaseous reaction products of Ti_2C, Ti_3C_2, Ti_3CN and Nb_2C MXenes in an aqueous environment (Fig. 5a) [24]. By comparing retention times, it can be clearly established that CH_4 is the predominant gaseous product of the degradation of all four MXenes in aqueous colloidal solutions. This suggests that carbide and carbonitride MXene converts carbon elemental to the gaseous product CH_4 during oxidative degradation. The composition of the gas products was further investigated in combination with Raman spectroscopy (Fig. 5b). The peaks at 2918 and 3020 cm^{-1} are assigned to the symmetric and asymmetric stretching vibrations of the C–H bond in CH_4, respectively, whereas the peak at 2331 cm^{-1} corresponds to the symmetric stretching vibration of N_2, which may be attributed to the dissolved air in the solution. The degree of oxidation of MXene can be assessed based on the amount of produced CH_4 gas.

Indirect evidence (*e.g.*, conductivity, electrochemical properties or pH values) has also been used to grossly detect degradation of MXene. Habib *et al.* detected the oxidation of $Ti_3C_2T_x$ in different media by conductivity measurements to evaluate the shelf life (Fig. 5c) [80]. For the oxidation of $Ti_3C_2T_x$ film in air, keeping for >2 months, the conductivity of the films changed from $2.49 \times 10^4 \pm 1.16 \times 10^3$ S/m to 4.90×10^2 S/m. Decrease in film conductivity indicates increased oxidation of MXene. Nevertheless, it is crucial to consider that MXene conductivity can be influenced by factors such as film thickness and MXene-layer alignment. Therefore, relying solely on a direct correlation between conductivity and oxidation may lead to erroneous interpretations. The electrochemical properties of layered $Ti_3C_2T_x$ film can also be used as an indicator of the oxidation degree [29]. During the first 20 h, the

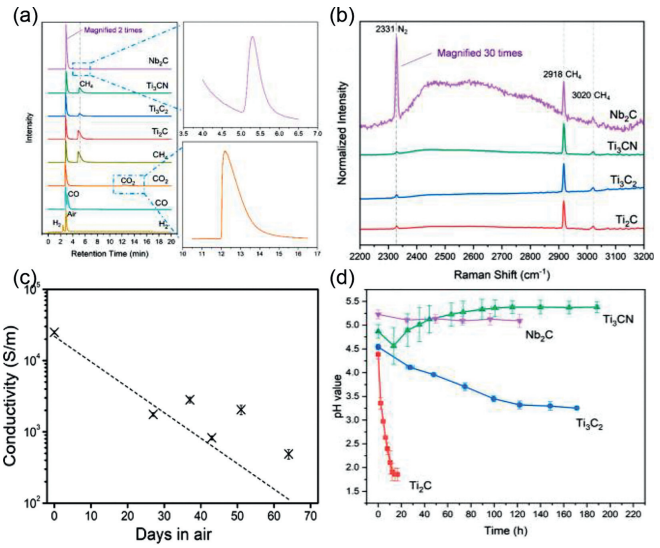

Fig. 5. (a) GC analysis of gaseous products of MXenes oxidation and standard gases. (b) Raman spectra of gas collected during MXenes transformations process in water. Reproduced with permission [24]. Copyright 2020, American Chemical Society. (c) Conductivity of MXenes film in air over time [80]. Reproduced with permission. Copyright 2019, Springer Nature. (d) Averaged pH values *vs.* time curve of MXene suspensions at 70 °C. Reproduced with permission [24]. Copyright 2020, American Chemical Society.

pH values of Ti_2C, Ti_3C_2, and Ti_3CN solutions gradually decreases, which may be attributed to the release of inserted acids (HF/HCl) during the degradation of the MXene (Fig. 5d). However, after a reaction time surpassing 20 h, the pH trend of the Ti_3CN solution changes from decreasing to increasing, which is significantly different from the other carbide MXene solutions, mainly due to the conversion of N element to ammonia during the carbonnitride MXene degradation. During the degradation of Nb_2C, there was no significant change in pH, which may indicate the low reactivity of Nb_2C in water. The rate of pH decrease corresponds to the degradation rate of the MXene material, and the oxidation of the MXene can be studied crudely by pH-monitoring experiments [24].

Although each technique can demonstrate MXene oxidation, it is not possible to determine the best analysis method. The characteristics of each respective technique have been summarized in Table 2. It is crucial to critically analyze the data acquired through different techniques. Instead of relying on a single technique to demonstrate oxidative process changes, we recommend the use of multiple techniques.

5. Factors affecting the oxidation of MXenes

To achieve the desired properties of MXenes for practical applications, it is essential to have a comprehensive understanding of the factors that influence their oxidative stability. The structural stability of MXenes is controlled by a number of key factors, both intrinsic and extrinsic, such as chemical composition, microstructure, surface functional groups, temperature, composition, and aqueous environment.

5.1. Intrinsic factors

The stability of MXenes is significantly influenced by their inherent chemical composition and microstructure. The "M" atom, "X" atom and the type and orientation of the termination groups largely determine the electronic properties of MXene. A surface chemistry analysis using XPS was conducted to investigate various types of MXenes including $Ti_3C_2T_x$, Ti_2CT_x, Ti_3CNT_x, Nb_2CT_x, and

Table 2
The summary of the characteristics of different methods employed for the detection of MXene oxidation.

Detection method	Advantages	Disadvantages
Visual assessment	Convenient color change observation linked to structural/compositional transformation	Variable outcomes Lacks quantitative assessment
UV–vis spectroscopy	Fast, non-destructive, quantitatively monitors colloidal oxidation degree Real-time monitoring Lifetime prediction Environmental factor evaluation	Limited to optical properties, may not provide detailed structural information
XRD	Directly observe the crystal structure and *d*-spacing during oxidation	Ineffective in detecting initially formed amorphous oxides
Raman spectroscopy	Sensitive to amorphous compounds and transition metal oxides	High laser power may cause sample oxidation
XPS	Sensitive to oxidation states Quantitative test of oxidation degree	Requires ultra-high vacuum Susceptible to surface contamination Costly instrumentation
SEM, TEM & EDS, EELS	Visualizes structural changes Atomic scale structure information	Limited to 2D observations Challenges in capture dynamic oxidation state changes in solution Requires specialized equipment and expertise
Gas analysis	Provides gaseous reaction product information, aids in understanding conversion mechanism	Structural transformation during oxidation cannot be directly observed
Indirect evidence	Simple to operate Low cost Short judgment cycle	Easily influenced by external factors, leading to erroneous interpretations

$Nb_4C_3T_x$. These MXenes exhibited different degrees of oxidation upon exposure to air, forming different amounts of oxidation products [81]. The thermodynamic stability of 54 MXene with the formula $M_{n+1}X_nO_2$ (M = Sc, Ti, V, Cr, Zr, Nb, Mo, Hf, Ta; X = C, N; $n = 1$, 2, 3) in solution were predicted through first-principles calculations. The fluorinate Sc-based MXene has been found to have the most excellent thermodynamic stability in aqueous environments [82]. Cr_2C may be unstable in aqueous solution, rapidly transforming to other phases such as chromium oxide [83]. Even for MXenes with similar chemical composition, the oxidative stability of MXenes is related to the number of MXene layers (n in $M_{n+1}X_nT_x$). MXenes with more layers (n) will have higher thermodynamic stability in aqueous solution, such as the oxidation rates trend: Ti_2CT_x > $Ti_3C_2T_x$ > $Ti_4C_3T_x$ [70,71,84]. This is attributed to the fact that they have much fewer exposed surfaces and fewer cationic vacancies and defects. N atoms will further strengthen the metallic properties of MXenes, thus carbonitrides and nitrides of MXene have stronger metallic properties than carbide MXene, which makes them more suitable as electrode materials. The binding energy of $Ti_{n+1}N_n$ is lower than that of the corresponding carbide, indicating that it has poor structural stability and is easily dissolved in aqueous solutions [60,85].

The high surface to volume ratio of MXene renders molecular or atomic groups that chemisorb onto its surface crucial for stability regulation [59,86]. During the preparation process, the removal of Al layer from the Ti_3AlC_2 MAX phase forms pure Ti_3C_2, which is an unstable material [87,88]. Pure Ti_3C_2 immediately reacts with water, acids or bases in the reaction system, leading to the formation of competing surface groups, such as -O, -F and -OH [30,89]. Additionally, during the aqueous etching process, even in the absence of external oxidizing agents (O_2 and H_2O), water molecules trapped between the MXene layers can induce surface oxidation [90]. The =O and -OH groups can also act as an oxidizing source to oxidize MXene [83]. The low-energy orbitals of the termination saturate the non-bonding valence electrons of the surface M atoms, which in turn will stabilize the MXene flake. Hu *et al*. predicted the stability of different groups terminated MXenes by manipulating the internal coordination of the octahedral crystal field to match the Cartesian coordination *via* orbital-resolved density of states analyses to accurately (Fig. 6a). The predicted stability order of $Ti_3C_2O_2$ > $Ti_3C_2F_2$ > $Ti_3C_2(OH)_2$ > $Ti_3C_2H_2$ > Ti_3C_2 agrees with the experimental results [87]. Organic molecules such as alkyl phosphonic acids [91], -$C_6H_3(CF_3)_2$ [92], β-mercaptoethanol [93], organic amines [94], are grafted onto the MXene surface can significantly enhance hydrolytic stability. The surface of MXene can be quite complex with one or some combination of OH, O, and F and other capping groups, and the proportions for each end group are also flexible and variable. Density functional theory (DFT) calculations show that the hydroxyl termination group is highly stable at 50% coverage, but is unstable at higher coverage [95]. Reducing the number of -OH terminations on the MXene surface improves its oxidation resistance [96]. There is still much to explore and discover regarding the effects of emerging surface terminations on MXene stability, which will aid in the design of MXenes with enhanced environmental stability.

In recent years, the importance of synthesizing high-quality MXenes with chemical and structural stability for practical applications in aqueous energy storage systems has been widely recognized. However, the use of harsh acid, LiF dosage in etching process, and excessive ultrasound power and time during ultrasonic processing to produce MXene NSs often leads to severe structural defects [66,97,98]. How LiF dosage in etching process affects the quality of MXene flakes is studied by electron microscopy technique (Fig. 6b). Although the structures of the flakes prepared by the two methods were the same (SAED patterns), there were obvious differences in their morphology. Flakes produced *via* Route 1 appeared smaller with uneven edges, decorated with tiny dark-colored particles (TiO_2), and displayed numerous pinhole defects. In contrast, flakes produced *via* Route 2 appeared larger with well-defined and clean edges, and no visible pinhole defects. These findings highlight the enhanced environmental stability and higher quality of $Ti_3C_2T_x$ flakes produced through Route 2, indicating the influence of etching solution composition on Al etching and Li^+ incorporation. Notably, the obtained multilayered $Ti_3C_2T_x$ flakes could be manually separated into single-layer flakes without the need for ultrasonic stripping, which reduces flake fragmentation into smaller pieces. Some of these defects are also inherited from the precursor MAX phases [99]. Low environmental stability of $Ti_3C_2T_x$ NSs can be attributed to the presence of numerous pinhole defects [97]. According to the oxidation mechanism of MXene, the defects are the sites foe the formation of metal oxide growth. These findings suggest that structural defects in MXene,

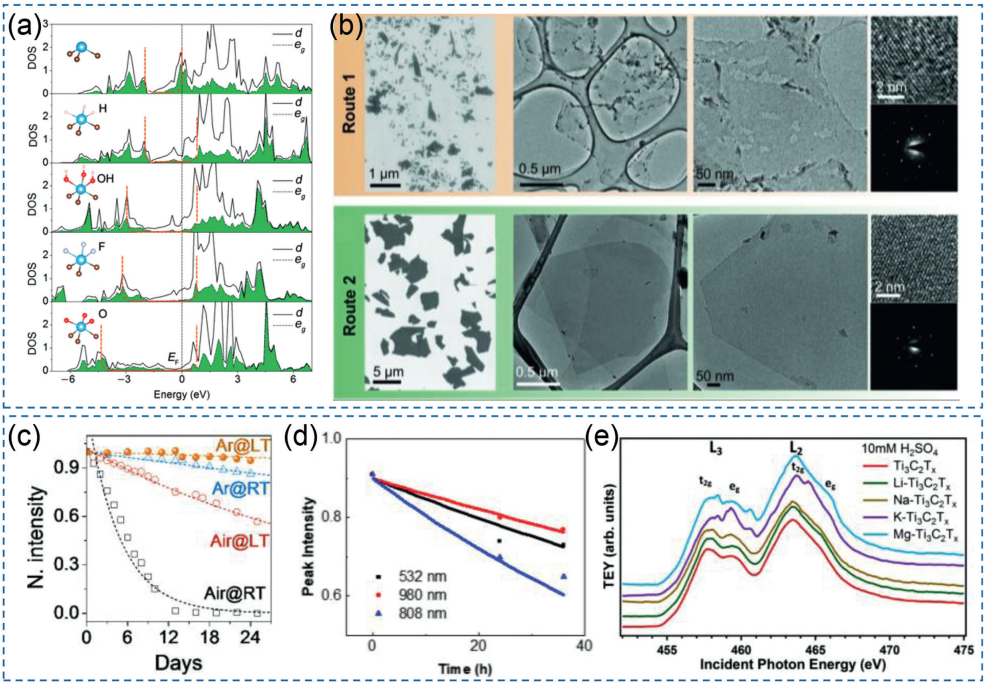

Fig. 6. (a) Pseudogaps of Ti2 3d orbitals in bare and terminated $Ti_3C_2T_2$ MXenes. Reproduced with permission [87]. Copyright 2017, American Chemical Society. (b) SEM and TEM images of MXene flakes produced through different routes Reproduced with permission [97]. Copyright 2016, Wiley Publishers. (c) Stability of MXene suspension in different environments (atmosphere and temperature). Reproduced with permission [69]. Copyright 2017, American Chemical Society. (d) Peak intensity *vs.* time curve using different continuous-wave lasers. Reproduced with permission [102]. Copyright 2019, American Chemical Society. (e) Ti L-edge XA spectra of pristine, ion intercalated MXene samples dispersed in 10 mmol/L H_2SO_4. Reproduced with permission [103]. Copyright 2020, American Chemical Society.

such as titanium vacancies, atomic steps, corrugations, and cavities, are important factors influencing MXene behavior in aqueous solutions, despite their inevitability. Furthermore, the formation of vacancies in MXenes is also influenced by the type of surface functional groups, with $Ti_3C_2T_x$ exhibiting lower vacancy formation energies for -F and -OH terminations compared to -O terminations [100,101]. The degradation process of MXene is flake size-dependent, with smaller flakes oxidizing faster than larger ones. $Ti_3C_2T_x$ MXene oxidation initiates at the flake edge and progresses inward, following a mono-exponential decay behavior [69]. $Ti_3C_2T_x$ suspension with low concentration and smaller flakes exhibit faster oxidation, primarily attributed to their high dispersion which exposes a larger surface area and more edges to H_2O/O_2. Conversely, high-concentration dispersions exhibited slow kinetics of oxidation, owing to the capping and steric shielding effects among the flakes [71].

5.2. Extrinsic factors

The storage environment (atmosphere, temperature and light) also affects the kinetics of the $Ti_3C_2T_x$ oxidation process. The delaminated-$Ti_3C_2T_x$ (d-$Ti_3C_2T_x$) MXene flakes exhibit instability when stored in ambient air atmosphere, as nearly all of the carbide undergoes oxidation to anatase titanium dioxide within 2 weeks. Sample stability was improved by injection of the inert gas Ar into the suspension, which was mainly attributed to the reduction of dissolved oxygen (Fig. 6c) [69]. In practical applications of aqueous energy storage devices, the ambient temperature is subject to variation and heats up due to operational heat release. Lowering the temperature significantly improves the time constant by nearly an order of magnitude (*e.g.*, from 4.8 days at room temperature to 42 days at 5 °C). Similarly, according to the Arrhenius equation, increasing the temperature promotes the oxidation rate. With the emerging applications of MXene in photocatalysis, photoelectronics, and photothermal conversion, it is crucial to investigate MXene stability under light irradiation. Laser irradiation accelerates the degradation of $Ti_3C_2T_x$ NSs by nearly 10-fold in the initial stage, generating smaller-sized oxidation products rapidly. This effect is primarily attributed to the surface plasmon resonance phenomenon of $Ti_3C_2T_x$ NSs (Fig. 6d) [102].

In the device configuration, the electrode material is infiltrated in the electrolyte, making the electrolyte pH, ionic species, and water activity influential factors in the oxidation kinetics of MXene. The effect of pH has already been discussed in the Oxidation Mechanism of MXenes section. The electronic structure of $Ti_3C_2T_x$ MXenes after Li^+, Na^+, K^+ and Mg^{2+} intercalation was investigated by XAS at the Ti L-edge. The oxidation state evolution of Ti atoms in $Ti_3C_2T_x$ MXenes was found to be cation-dependent (Fig. 6e) [103]. Both dissolved oxygen and water molecules play pivotal roles in the destruction of the MXene structure. The use of chemical hydration of inorganic salts with smaller anionic and cationic radii and weaker coordination of metal ions such as LiCl, NaCl, and $CaCl_2$ can reduce the proportion of free water molecules in solution as well as oxygen solubility, which can effectively extend the storage life of MXene [33].

$Ti_3C_2T_x$ undergoes irreversible oxidation relative to Ag/AgCl at around 450 mV to form TiO_2 nanoclusters [104]. This strongly alters its surface properties at the electrode potentials required for OER. Therefore, stabilizing MXenes in this potential range is a serious challenge to be addressed in the future.

6. Strategies to mitigate oxidation of MXenes

The oxidative stability of MXenes in aqueous solution is critical to their broad applicability. From the preceding discussion, it can be concluded that the oxidation of MXene in aqueous solutions is a multifaceted process that is intricately affected by various factors working in synergy. There is an urgent need to produce MXenes or non-aqueous MXenes devices with good environmental stability, and therefore there is an urgent need to investigate methods

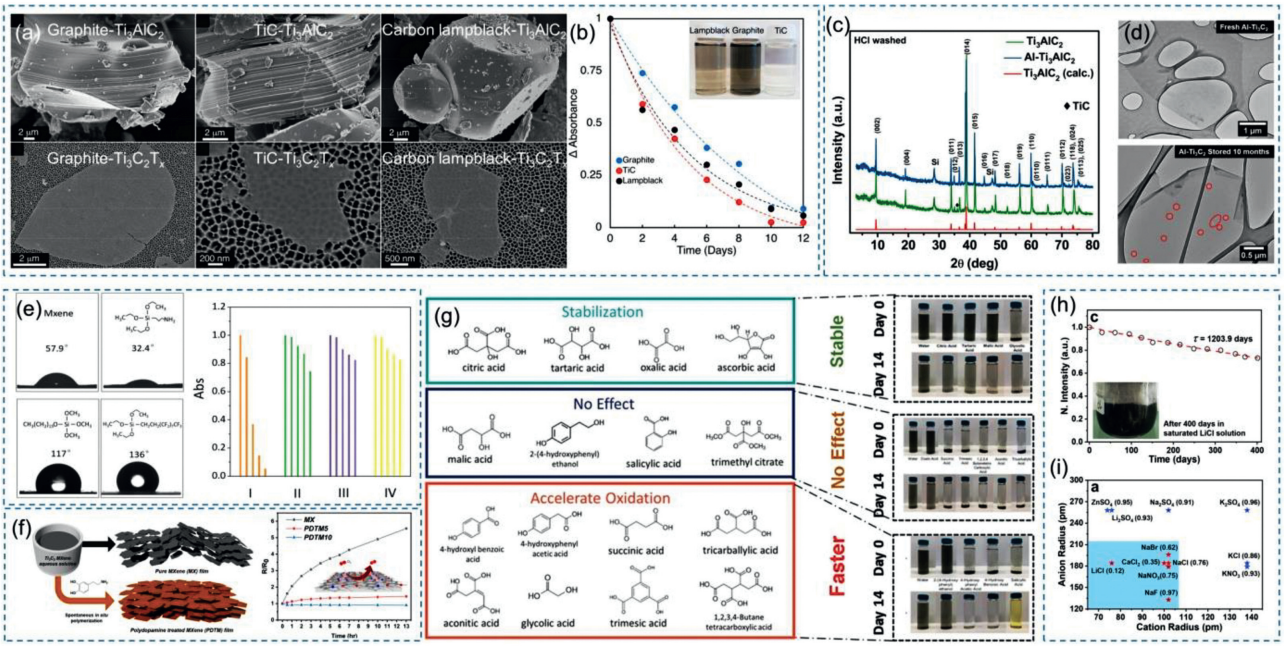

Fig. 7. (a) SEM images of Ti_3AlC_2 synthesized by graphite, TiC, and carbon lampblack as carbon source and corresponding MXene produced *via* MILD method. Reproduced with permission [106]. Copyright 2019, American Chemical Society. (b) Solution stability of the MXene suspensions. (c) XRD patterns of Ti_3AlC_2 and Al-Ti_3AlC_2. Reproduced with permission [34]. Copyright 2021, American Chemical Society. (d) TEM images Al-Ti_3C_2 flake before and after 10 months storage. (e) Contact angle measurements and normalized UV–vis absorbance of MXene and silylation-functioned MXenes after different storage time (0, 1, 3, 6, and 11 days). Reproduced with permission [115]. Copyright 2019, Elsevier. (f) Schematic of polydopamine-treated MXene (PDTM) film synthesis and ambient stability *via* electrical resistance change upon heating (170 °C) in air. Reproduced with permission [116]. Copyright 2020, American Chemical Society. (g) Effect of various antioxidants on $Ti_3C_2T_x$ stability. Reproduced with permission [58]. Copyright 2023, Springer Nature. (h) Stability of $Ti_3C_2T_x$ stored in saturated LiCl solution. Reproduced with permission [33]. Copyright 2021, Wiley Publishers. (i) Water activity of saturated solution of various inorganic salts with different cation and anion radii, the salts in the blue shaded area effectively reduce the water activity and protect MXene from oxidation.

to mitigate the oxidation and degradation of MXenes. Current research efforts are focused on three aspects: optimization of synthetic routes, isolation of MXene from H_2O and O_2 contact, and modification the electronic structure.

6.1. Optimization of synthetic routes

It was concluded that high-quality (fewer defects and larger lateral dimensions) MXenes are more chemically stable because the structural defects and edge sites are oxidative nucleation sites [66,97,105]. Most experimentally synthesized MXenes are produced by the etching of MAX phases, and these MAX structural and stoichiometric features are ultimately translated into the morphology and behavior of the MXene. Examples include defects on the atomic scale, and MAX grain size and shape on the micro/macro scale. The use of different titanium sources (Ti, TiH_2, or TiO_2), carbon precursors (TiC, graphite, Al_4C_3, or carbon lampblack), and various synthesis methods (such as hot isostatic pressing, high-temperature annealing, self-propagating high-temperature synthesis, or spark plasma sintering) significantly influence the MAX microstructures, phase compositions, grain sizes, and resulting properties. For instance, in synthesizing Ti_3AlC_2, the precursor for $Ti_3C_2T_x$ MXene, three carbon sources (graphite, TiC, and carbon lampblack) were employed (Figs. 7a and b). Differences in the grain size of the synthesized Ti_3AlC_2 were found through SEM images, with both graphite and TiC sources yielding larger crystals with a lamellar morphology, whereas the crystals produced by carbon lampblack yielded smaller crystals. There were also differences in the size of the MXene flakes produced through the MILD process: graphite-MXene > TiC-MXene > carbon lampblack-MXene. The obtained products showed differences in chemical stability in aqueous solution. The time constant of $Ti_3C_2T_x$ derived from graphite was significantly larger (10.1 days), whereas TiC and carbon lampblack produced $Ti_3C_2T_x$ samples displayed a time constant of 4–5 days. Notably, the graphite samples exhibited the largest lateral size, leading to the slowest degradation rate [106]. It is generally accepted that a pure phase of MAX should yield the highest quality MXene, and most current MAX synthesis schemes use well-established synthesis protocols that result in minimal doping of the sintered product. In fact, Mathis *et al.* discovered that the addition of excess Al during high-temperature synthesis of the MAX phase resulted in Ti_3AlC_2 grains with improved structural ordering and a high carbon stoichiometry (Fig. 7c) [34]. The derived MXene NSs (Al-Ti_3C_2) were of high quality, with only a few pinholes appearing on the flakes after ten months (Fig. 7d). The aqueous suspensions of Al-Ti_3C_2 NSs demonstrated a shelf life of over ten months, whereas the previously published Ti_3C_2 for only 1–2 weeks.

Etching the MAX phase using mixed etching acids (*e.g.*, LiF/HCl, HCl/HF, $(CH_3)_4NF$/HCl) or using bifluorides (*e.g.*, NH_4HF_2) instead of pure HF, the chemical stability of the synthesized MXene was enhanced due to the reduced concentration of defects [41,97,107,108] In addition, etching time, temperature, exfoliation Methods (sonication, power-focused delamination, minimally intensive layer delamination MILD), and ultrasonication time all have an effect on the quality of synthesized MXene [41,109–111]. For instance, when etching the MAX phase using the LiF/HCl method, high LiF concentration leads to the formation of vacancy defects [97]. In addition, ultrasonic processing can form many vacancy defects on the MXene surface [58]. The delamination process utilizing organic molecules such as TBA^+ or TMA^+ can contribute to defect formation, and this effect might have a greater impact compared to harsh etching conditions [112]. To mitigate this issue, a LiCl ion exchange/flocculation technique was implemented as a post-treatment method to replace TBA^+ or TMA^+ with Li^+ ions. The degradation time of V_2CT_x MXene in aqueous solution increased

from hours to months after treatment [75]. The surface termination affects the oxidation resistance of MXene NSs (discussed in Section 5.1), while the surface termination is highly related to the preparation method and the reagents employed for the initial etching of the MAX phase [31,52]. Moreover, reducing the number of -OH terminations *via* hydrogen annealing method can effectively improve the stability of MXene films [96]. However, the annealed films displayed inferior redispersibility in aqueous solution, which has a negative impact on the subsequent modification treatment and the performance of aqueous energy storage devices. The continuous development of MAX precursors and the optimization of the synthesis protocol of MXenes are important for obtaining MXenes with high oxidation resistance.

6.2. Isolation of MXene from H_2O and O_2 contact

It is known that water and dissolved oxygen are oxidizing agents for MXene oxidation, so isolating water molecules and oxygen molecules from the surface of MXene naturally slows down the rate of MXene degradation in aqueous solutions. To inhibit the contact of MXenes with H_2O/O_2 molecules in aqueous solution, researchers proposed strategies to incorporate materials with high chemical stability into MXenes, including carbon nanoplating, transition metal dichalcogenides, organic acids, and polymers [65,84,113,114]. Different kinds of silylation reagents are tightly attached to the surface of MXene through covalent bonding, which can effectively inhibit the structural degradation caused by the oxidation of MXene [115]. From Fig. 7e, it can be seen that the antioxidant capacity of functionalized MXene is closely related to its hydrophilicity, and (3-aminopropyl)triethoxysilane is considered as a homogeneous protective layer obstructing the direct contact of H_2O/O_2 with MXene. Enhancing the hydrolysis resistance of MXene by sacrificing its hydrophilicity can have a detrimental effect on its performance in aqueous energy storage systems. To address this issue, Wu *et al*. proposed a carbon nanoplating strategy that effectively curbs surface oxidation and structural degradation of MXenes during synthesis and catalysis [65]. The strategy involves the uniform deposition of a conductive carbon layer with a thickness of a few nanometers onto the MXene surface, creating a thin physical barrier that restricts the inward diffusion of oxygen into the MXene lattice. Another approach involves the direct uniform coating of the MXene surface with ultrathin polymer layers *via* a simple polymerization reaction. For instance, dopamine monomers can undergo spontaneous oxidative polymerization on the MXene surface, resulting in ideal parallel stacking of MXene films. This method significantly enhances oxidation resistance without compromising the original high electrical conductivity of MXene (Fig. 7f) [116]. After aging at high temperatures for 13 h, the resistance of pure MXene film increased by more than five times, while the PDTM5 film showed a much smaller increase. This is mainly attributed to the effective screening of the polydopamine layer against oxygen and moisture in the environment.

Since oxidation starts from surface edge defects and extends towards the interior of the whole MXene flake, surface passivation of these defects is an effective way to inhibit MXene hydrolysis. MXene surfaces are negatively charged while their edges are positively charged. Zhao *et al*. demonstrated that hydrolysis can be suppressed by adding sodium L-ascorbate (NaAsc) as an antioxidant to $Ti_3C_2T_x$ colloids [117]. Molecular dynamic simulations revealed that the ascorbate anions preferentially absorbed at the edges, providing steric shielding that restricted water molecules from reaching reactive sites. The NaAsc-stabilized dispersions were stable for 21 days in closed containers and the amount of small molecule antioxidants needed to cover the MXene edge is relatively large. Natu *et al*. encapsulated the edges of the $Ti_3C_2T_x$ and V_2CT_x MXene flakes with economical and environmentally friendly polyanions, such as polyphosphates, polysilicates, or polyborates (Fig. 1 isolation of MXene from H_2O and O_2 contact) [35]. It was found that a concentration of only 0.1 mol/L was sufficient to inhibit MXene oxidation for at least 3 weeks in aerated water at ambient temperature. The passivation process follows a simple ionic interaction mechanism, where the negatively charged oxygen functional groups of the anions effectively interact with the positively charged edges of the MXenes, acting like a cap and preventing contact with H_2O/O_2. However, the specific nature of these interactions between antioxidants and MXene remains unclear, which hinders the future selection and design of highly stable MXenes. Zhao *et al*. systematically investigated the effects of three classes of organic antioxidant candidates, α–hydroxy acids, polycarboxylic acids and phenols, on the oxidative stability of $Ti_3C_2T_x$ and Ti_2CT_x (Fig. 7g) [84]. Oxidative stability was assessed by testing the Ti^{4+} content of NSs during 14 days storage. It was observed that certain antioxidants did not provide protection to MXene, and in fact, some even accelerated degradation, such as polycarboxylic acids and phenolic compounds. Citric and tartaric acids exhibit efficacy in MXene stabilization by virtue of their capacity to form stable five or six-membered chelation rings with Ti, thereby inhibiting water interactions. Conversely, malic and glycolic acids demonstrate diminished effectiveness attributable to their limited coordinating groups and inability to establish stable ring structures. Tricarballylic acid and trimethyl citrate are rendered ineffective for chelation due to the absence of hydroxyl groups or the formation of unfavorable ring geometries. Oxalic acid stands out as effective, leveraging its established chelating prowess to create a stable 5-membered ring, whereas succinic acid is less effective, forming a less favorable 7-membered ring. The efficacy of antioxidants hinges on a constellation of factors, including the number of chelation coordination sites, molecular chain length, and the stability of the resulting chelation complexes.

To achieve efficient stabilization of MXene in aqueous solution, the hydration effect of salt is utilized to bind free water molecules and reduce water activity and dissolved oxygen concentration [33]. After 400 days of storage in saturated LiCl solution, the proportion of Ti-O species in MXene only increased to 16.8% compared to fresh samples, which was very effective in stabilizing MXene in solution, even it significantly prolonged the antioxidant time constant (τ) to 1203.9 days (Fig. 7h). It was also found that LiCl, NaCl, $CaCl_2$ all could efficiently stabilize MXene in aqueous solution. These findings highlight the potential of water activity as an indicator for guiding the screening of salt protectants for MXene stabilization. Inorganic salts composed of cations with ionic radii below 102pm (*e.g.*, Li^+, Na^+, Ca^{2+}, Zn^{2+}) and anions with ionic radii below 196pm (*e.g.*, F^-, Cl^-, Br^-, NO_3^-, OH^-) tend to exhibit lower water activity and can better stabilize MXene (Fig. 7i). This is mainly due to the stronger ion-dipole interaction between smaller ions and water molecules, which will effectively bind free water molecules, effectively binding free water molecules and inhibiting the attack of H_2O/O_2 on MXene.

Changes in storage conditions (deaeration and lower temperature) can also extend the shelf life of MXene by reducing the reactivity of water and oxygen molecules. Storing MXene suspension at low temperatures (−18 °C and −80 °C) significantly extends its shelf life due to slower oxidation kinetics. However, it should be noted that even at 5 °C, severe oxidation can still occur, making this method energy-intensive [118].

6.3. Modification the electronic structure

Previous studies have shown that H_2O rather than O_2 plays a critical role in the degradation of MXene NSs in aqueous solution [70]. First-principles molecular dynamics simulations have further confirmed that MXene is more vulnerable to water attack due to

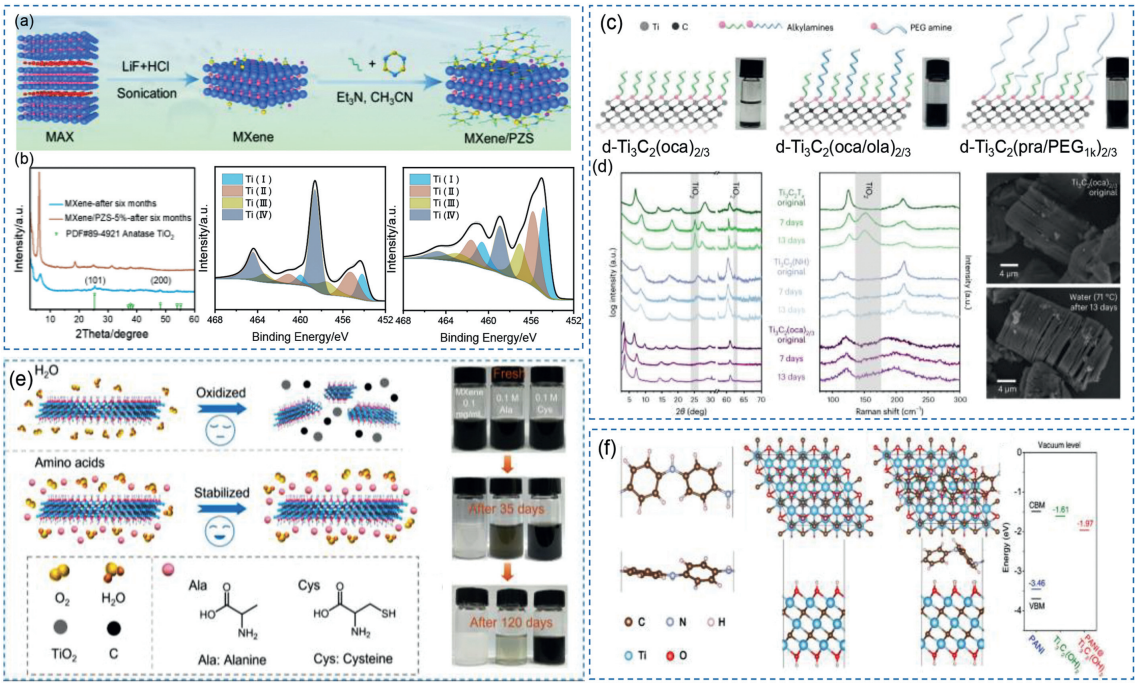

Fig. 8. (a) Schematics of the MXene/PZS fabrication process. Reproduced with permission [36]. Copyright 2023, Elsevier. (b) XRD patterns and XPS spectra of pure MXene and MXene/PZS-5% after 6 months of storage. (c) Schematics of delaminated h-MXenes with different types of surface ligands. Reproduced with permission [94]. Copyright 2023, Springer Nature. (d) XRD, Raman spectra and SEM images h-MXenes after different exposure time. (e) Environmental stability of MXene enhanced by alanine and cysteine. Reproduced with permission [120]. Copyright 2023, Wiley Publishers. (f) Work functions of PANI, $Ti_3C_2(OH)_2$, and PANI@$Ti_3C_2(OH)_2$. Reproduced with permission [122]. Copyright 2019, Wiley Publishers.

the chemisorption of water molecules on the surface of Ti atoms, which leads to the formation of Ti-OH species [119]. Altering the electronic structure of surface M atoms has proven to be an effective approach in enhancing the chemical stability of MXene. Polymers, small organic molecules, and ions incorporated with MXene, in addition to the physical shielding effect of isolating H_2O/O_2 contact, will also have charge transfer with MXene, affecting the electronic structure of MXene to enhance its antioxidant properties [36,93,94,120]. Chemical modification strategies have a wide range of uses in controlling the chemical and electronic properties of MXenes. Li *et al.* demonstrated a successive condensation reaction to fabricate cyclocrosslinked polyphosphazene modified MXene (MXene/PZS) by forming the Ti-O-P covalent bond (Fig. 8a) [36]. After 6 months of storage, XRD analysis revealed the appearance of new peaks corresponding to anatase TiO_2 in the spectra of pure MXene, while no such peaks were observed in the MXene/PZS-5% spectra (Fig. 8b). The Ti^{4+} content in MXene/PZS only increased from 11.43% to 19.33% after aging, in contrast to the significant increase from 9.6% to 50.14% observed in pure MXene. DFT calculations and XPS analysis indicated that PZS donates electrons to the MXene surface through Ti-O-P bonds, effectively inerting the Ti atoms and slowing down the surface transformation process. Interactions between small organic molecules and MXene also influence the hydrolytic stability. Zhou *et al.* synthesized a class of heterogeneous MXenes (h-MXenes) using the reaction of halogenated MXenes with organic amines, forming amine and imine bonds between the organic and inorganic portions (Fig. 8c). After aging at high temperature (at 71 °C), it was found that the $Ti_3C_2T_x$ samples formed anatase-type TiO_2 phases after 7 days, while no such phases were detected in $Ti_3C_2(NH)$ and h-MXene samples even up to 13 days (Fig. 8d). SEM images of $Ti_3C_2(oca)_{2/3}$ before and after exposure to pure water at 71 °C for 13 days revealed no significant differences, with no TiO_2 nanoparticles observed on the surface. Additionally, h-MXenes exhibited improved stability in KOH solution. Comparative tests indicated that in addition to the hydrophobic barrier provided by alkyl chains, the enhanced hydrolytic stability of amine/imide terminated MXenes can be attributed to the reduced susceptibility of surface titanium atoms to nucleophilic attack by hydroxyl ions [94]. Moreover, a synergistic strategy of forming hydrogen bonds (H bonds) and coordination bonds has been employed to improve the chemical stability of $Ti_3C_2T_x$ MXene in aqueous solutions (Fig. 8e) [120]. The 2D layered and crystalline structures of alanine hydrogen bonding-modified $Ti_3C_2T_x$ can be preserved for not <35 days, while the cysteine hydrogen bonding and coordination bonding synergistically modified $Ti_3C_2T_x$ can even be maintained for not <120 days. Both alanine and cysteine molecules inhibit MXene oxidation by forming both hydrogen and Ti-S bonds with MXene that occupy the reaction site and resist attack by water molecules. Cysteine molecules exhibited more effective inhibition on the oxidation of $Ti_3C_2T_x$, attributed to the synergistic effect of Ti-S and H bonds. However, it is still necessary to further investigate the relationship between the types of interaction forces and the hydrolytic stability, in order to lay the foundation for the synthesis of high-stability MXenes.

The doping of certain non-metallic elements into MXene materials can effectively increase the bonding energy between atoms in the materials and thus improve the stability of MXene [23,121]. MXene is easy to oxidize at anodic oxidation potential, and they are often used as negative electrodes. Hierarchical polyaniline@MXene was prepared by casting a uniform polyaniline layer on a 3D porous $Ti_3C_2T_x$ MXene. Compared with $Ti_3C_2T_x$ MXene, first-principles calculations show that the PANI@MXene heterostructure has a larger work function (Fig. 8f), resulting in enhanced oxidation electrochemical stability at higher anodic potentials, so it can be used as a stable anode material and exhibits an ultrahigh volume specific capacitance [122]. Recently, MXene nanosheets have been assembled into a layered structure mediated by alkali metal cations for energy storage applications. This cation-driven assembly not only significantly improves the electrochemical performance of MXenes but also transforms chem-

ically/electrochemically unstable MXene flakes into highly stable thin films and electrodes. The inhibition of oxidation is related to the charge transfer from the inserted alkali ions into MXene nanosheets [123,124]. The Al^{3+} intercalated MXene was found to have excellent long-term stability in aqueous environments up to 400 h. DFT theoretical calculations revealed that Al^{3+} was able to have strong interactions with the oxygen groups on the surface of the MXene NSs, which enabled the MXene films to maintain good structural stability in aqueous solutions [125].

7. Summary and outlook

The distinctive morphology, mechanical characteristics, and electronic properties of MXenes have generated substantial enthusiasm for the advancement of MXenes-based aqueous energy storage devices. Nevertheless, the environmental instability of MXenes presents a notable hurdle in their processing and commercial implementation. The presence of oxygen, water, and light can lead to the conversion of MXenes into oxides, resulting in the deterioration of their 2D lamellar structure. This transformation process has a detrimental impact on the structural integrity, electronic structure, and performance of MXenes.

Studies have previously conducted investigations on the oxidation of MXenes, specifically focusing on $Ti_3C_2T_x$, under various storage conditions. These studies have identified multiple parameters that impact the oxidation rate. These parameters encompass intrinsic properties, size, and concentration of MXenes, dispersion pH, cationic species, and dispersion concentration. It has been recognized that surface defects, edges, and vacancies within MXenes are particularly vulnerable to oxidation. Hence, the elimination of surface defects, whether inherited from the MAX phase or generated during mechanical and chemical stripping, has the potential to enhance the oxidative stability of MXenes. Nevertheless, a comprehensive understanding regarding the interaction between water molecules and these susceptible sites remains limited. The development of *in-situ* techniques is necessary to examine the morphological and electronic alterations during the oxidation process at a microscopic level.

Precise management of defect sites plays a crucial role in mitigating the oxidation of MXenes. It is essential to exercise precise control over the presynthesis conditions, such as the quality of the MAX phase, as well as the synthesis conditions. These practices can effectively slow down the oxidation process in MXenes. Therefore, it becomes imperative to establish scalable and environmentally friendly synthesis protocols that yield high-quality MXenes. Moreover, a more profound comprehension of MXene crystal structures, functionality, and atomic defects is necessary. This can be accomplished by optimizing synthetic schemes to ensure maximum stability. Currently, existing knowledge about these characteristics often relies on empirical observations, lacking solid theoretical mechanisms.

The oxidation mechanism of $Ti_3C_2T_x$ in aqueous energy storage systems remains subject to ongoing controversy, primarily due to the complexity and variability of its environment. The oxidation process is influenced by several competing reactions, including atom attachment, water trapping, and edge oxidation. It is crucial to establish a solid foundation to understand the correlation between surface or edge-related chemistry and the behavior of most MXenes in different environmental conditions. Current indicators used to approximate MXene oxidation, such as changes in color and electrical conductivity, may not accurately reflect the true oxidation state. Hence, there is a need to develop novel techniques that enable precise identification and quantification of the extent of MXene oxidation. This, naturally, requires the advancement of *in-situ* methodologies capable of capturing comprehensive microscopic details of MXene states.

Various antioxidant methods have been developed to stabilize MXenes in aqueous solutions, primarily focusing on Ti-based MXenes. Each method has its own advantages and drawbacks. For instance, controlling the storage environment can significantly prolong the storage time of MXenes, yet it does not fundamentally enhance their oxidative stability. Modified synthesis approaches can enhance MXene's oxidative stability by reducing surface defect density, but they only slow down the oxidation rate without addressing the root cause of oxidation. Doping, although capable of improving MXene stability at the fundamental level, can lead to significant damage to MXene morphology and the introduction of pore defects. Therefore, comprehensive research is needed to make informed choices in selecting antioxidant methods based on practical applications.

Declaration of competing interest

The authors declare that they have no known competing financial interests or personal relationships that could have appeared to influence the work reported in this paper.

CRediT authorship contribution statement

Li Li: Investigation, Visualization, Writing – original draft. **Xue Ke:** Visualization, Writing – review & editing. **Shan Wang:** Writing – review & editing. **Zhuo Jiang:** Funding acquisition, Resources. **Yuzheng Guo:** Resources, Supervision, Writing – review & editing. **Chunguang Kuai:** Conceptualization, Supervision, Writing – review & editing, Funding acquisition.

Acknowledgments

This work was supported by the Fundamental Research Funds for the Central Universities (No. 2042023kf0094), the National Key Research and Development Program of China (No. 2022YFA1502902), the National Natural Science Foundation of China (No. 22101217).

References

[1] Z. Yang, J. Zhang, M.C.W. Kintner-Meyer, et al., Chem. Rev. 111 (2011) 3577–3613.
[2] C. Li, S. Jin, L.A. Archer, et al., Joule 6 (2022) 1733–1738.
[3] M. Huang, X. Wang, X. Liu, et al., Adv. Mater. 34 (2022) 2105611.
[4] J. Peng, W. Zhang, S. Wang, et al., Adv. Funct. Mater. 32 (2022) 2111720.
[5] Y. Zhu, S. Zheng, P. Lu, et al., Natl. Sci. Rev. 9 (2022) nwac024.
[6] L. Kong, M. Cheng, H. Huang, et al., EnergyChem 4 (2022) 100090.
[7] J. Jia, Y. Zhu, P. Das, et al., J. Materiomics 9 (2023) 1242–1262.
[8] X. Li, Z. Huang, C.E. Shuck, et al., Nat. Rev. Chem. 6 (2022) 389–404.
[9] A. Djire, H. Zhang, J. Liu, et al., ACS Appl. Mater. Interfaces 11 (2019) 11812–11823.
[10] Y. Zhu, S. Wang, J. Ma, et al., Energy Stor. Mater. 51 (2022) 500–526.
[11] T. Zhang, C.E. Shuck, K. Shevchuk, et al., J. Am. Chem. Soc. 145 (2023) 22374–22383.
[12] Y. Zhu, J. Ma, P. Das, et al., Small Meth. 7 (2023) 2201609.
[13] Y. Zhao, J. Zhang, X. Guo, et al., Chem. Soc. Rev. 52 (2023) 3215–3264.
[14] A. Gentile, S. Marchionna, M. Balordi, et al., ChemElectroChem 9 (2022) e202200891.
[15] F. Shahzad, M. Alhabeb, C.B. Hatter, et al., Science 353 (2016) 1137–1140.
[16] X. Xiao, H. Yu, H. Jin, et al., ACS Nano 11 (2017) 2180–2186.
[17] X. Liu, F. Xu, Z. Li, et al., Coordin. Chem. Rev. 464 (2022) 214544.
[18] F. Cao, Y. Zhang, H. Wang, et al., Adv. Mater. 34 (2022) e2107554.
[19] M. Han, D. Zhang, C.E. Shuck, et al., Nat. Nanotechnol. 18 (2023) 373–379.
[20] A. Vahid Mohammadi, J. Rosen, Y. Gogotsi, Science 372 (2021) eabf1581.
[21] Z. Zhang, F. Zhang, H. Wang, et al., J. Mater. Chem. C 5 (2017) 10822–10827.
[22] Z. Zheng, C. Guo, E. Wang, et al., Inorg. Chem. Front. 8 (2021) 2164–2182.
[23] J. Jiang, S. Bai, J. Zou, et al., Nano Res. 15 (2022) 6551–6567.
[24] S. Huang, V.N. Mochalin, ACS Nano 14 (2020) 10251–10257.
[25] R.A. Soomro, P. Zhang, B. Fan, et al., Nano-Micro Lett. 15 (2023) 108.
[26] F. Xia, J. Lao, R. Yu, et al., Nanoscale 11 (2019) 23330–23337.
[27] P. Hou, Y. Tian, Y. Xie, et al., Angew. Chem. Int. Ed. 62 (2023) e202304205.
[28] S. Doo, A. Chae, D. Kim, et al., ACS Appl. Mater. Interfaces 13 (2021) 22855–22865.
[29] J. Tang, T.S. Mathis, N. Kurra, et al., Angew. Chem. Int. Ed. 58 (2019) 17849–17855.

[30] M. Naguib, V.N. Mochalin, M.W. Barsoum, et al., Adv. Mater. 26 (2014) 992–1005.
[31] J. Zou, J. Wu, Y. Wang, et al., Chem. Soc. Rev. 51 (2022) 2972–2990.
[32] W. Peng, M. Luo, X. Xu, et al., Adv. Energy Mater. 10 (2020) 2001364.
[33] X. Wang, Z. Wang, J. Qiu, Angew. Chem. Int. Ed. 60 (2021) 26587–26591.
[34] T.S. Mathis, K. Maleski, A. Goad, et al., ACS Nano 15 (2021) 6420–6429.
[35] V. Natu, J.L. Hart, M. Sokol, et al., Angew. Chem. Int. Ed. 58 (2019) 12655–12660.
[36] L. Li, H. Niu, J. Robertson, et al., Electrochim. Acta 439 (2023) 141574.
[37] Y. Fan, L. Li, Y. Zhang, et al., Adv. Funct. Mater. 32 (2022) 2111357.
[38] M. Hu, H. Zhang, T. Hu, et al., Chem. Soc. Rev. 49 (2020) 6666–6693.
[39] M. Naguib, M. Kurtoglu, V. Presser, et al., Adv. Mater. 23 (2011) 4248–4253.
[40] M. Naguib, O. Mashtalir, J. Carle, et al., ACS Nano 6 (2012) 1322–1331.
[41] M. Alhabeb, K. Maleski, B. Anasori, et al., Chem. Mater. 29 (2017) 7633–7644.
[42] A. Feng, Y. Yu, Y. Wang, et al., Mater. Des. 114 (2017) 161–166.
[43] M. Ghidiu, M.R. Lukatskaya, M.Q. Zhao, et al., Nature 516 (2014) 78–81.
[44] F. Liu, A. Zhou, J. Chen, et al., Appl. Surf. Sci. 416 (2017) 781–789.
[45] X. Wang, C. Garnero, G. Rochard, et al., J. Mater. Chem. A 5 (2017) 22012–22023.
[46] X. Xie, Y. Xue, L. Li, et al., Nanoscale 6 (2014) 11035–11040.
[47] G. Zou, Q. Zhang, C. Fernandez, et al., ACS Nano 11 (2017) 12219–12229.
[48] T. Li, L. Yao, Q. Liu, et al., Angew. Chem. Int. Ed. 57 (2018) 6115–6119.
[49] S.Y. Pang, Y.T. Wong, S. Yuan, et al., J. Am. Chem. Soc. 141 (2019) 9610–9616.
[50] M.R. Lukatskaya, J. Halim, B. Dyatkin, et al., Angew. Chem. Int. Ed. 53 (2014) 4877–4880.
[51] W. Sun, S.A. Shah, Y. Chen, et al., J. Mater. Chem. A 5 (2017) 21663–21668.
[52] S. Yang, P. Zhang, F. Wang, et al., Angew. Chem. Int. Ed. 57 (2018) 15491–15495.
[53] P. Urbankowski, B. Anasori, T. Makaryan, et al., Nanoscale 8 (2016) 11385–11391.
[54] M. Li, J. Lu, K. Luo, et al., J. Am. Chem. Soc. 141 (2019) 4730–4737.
[55] Y. Li, H. Shao, Z. Lin, et al., Nat. Mater. 19 (2020) 894–899.
[56] M. Zhang, R. Liang, N. Yang, et al., Adv. Energy Mater. 12 (2021) 2102493.
[57] S. Kajiyama, L. Szabova, H. Iinuma, et al., Adv. Energy Mater. 7 (2017) 1601873.
[58] P. Huang, W.Q. Han, Nano-Micro Lett. 15 (2023) 68.
[59] V. Kamysbayev, A.S. Filatov, H. Hu, et al., Science 369 (2020) 979–983.
[60] I.R. Shein, A.L. Ivanovskii, Comp. Mater. Sci. 65 (2012) 104–114.
[61] L. Liu, H. Zschiesche, M. Antonietti, et al., Adv. Energy Mater. 13 (2023) 2202709.
[62] C. Xu, L. Wang, Z. Liu, et al., Nat. Mater. 14 (2015) 1135–1141.
[63] D. Wang, C. Zhou, A.S. Filatov, et al., Science 379 (2023) 1242–1247.
[64] R.B. Rakhi, B. Ahmed, M.N. Hedhili, et al., Chem. Mater. 27 (2015) 5314–5323.
[65] X. Wu, Z. Wang, M. Yu, et al., Adv. Mater. 29 (2017) 1607017.
[66] K.R.G. Lim, M. Shekhirev, B.C. Wyatt, et al., Nat. Syn. 1 (2022) 601–614.
[67] M.A. Hope, A.C. Forse, K.J. Griffith, et al., Phys. Chem. Chem. Phys. 18 (2016) 5099–5102.
[68] R. Lotfi, M. Naguib, D.E. Yilmaz, et al., J. Mater. Chem. A 6 (2018) 12733–12743.
[69] C.J. Zhang, S. Pinilla, N. McEvoy, et al., Chem. Mater. 29 (2017) 4848–4856.
[70] S. Huang, V.N. Mochalin, Inorg. Chem. 58 (2019) 1958–1966.
[71] X. Zhao, A. Vashisth, J.W. Blivin, et al., Adv. Mater. Interfaces 7 (2020) 2000845.
[72] L. Lorencova, T. Bertok, E. Dosekova, et al., Electrochim. Acta 235 (2017) 471–479.
[73] K. Hantanasirisakul, Y. Gogotsi, Adv. Mater. 30 (2018) 1804779.
[74] J. Kim, Y. Yoon, S.K. Kim, et al., Adv. Funct. Mater. 31 (2021) 2008722.
[75] K. Matthews, T. Zhang, C.E. Shuck, et al., Chem. Mater. 34 (2021) 499–509.
[76] M. Zhang, F. Héraly, M. Yi, et al., Cell Rep. Phys. Sci. 2 (2021) 100449.
[77] L. Yang, D. Kan, C. Dall'Agnese, et al., J. Mater. Chem. A 9 (2021) 5016–5025.
[78] A. Sarycheva, Y. Gogotsi, Chem. Mater. 32 (2020) 3480–3488.
[79] M. Peng, L. Wang, L. Li, et al., Adv. Funct. Mater. 32 (2022) 2109524.
[80] T. Habib, X. Zhao, S.A. Shah, et al., npj 2D Mater. Appl. 3 (2019) 8.
[81] J. Halim, K.M. Cook, M. Naguib, et al., Appl. Surf. Sci. 362 (2016) 406–417.
[82] M. Ashton, K. Mathew, R.G. Hennig, et al., J. Phys. Chem. C 120 (2016) 3550–3556.
[83] B. Anasori, M.R. Lukatskaya, Y. Gogotsi, Nat. Rev. Mater. 2 (2017) 16098.
[84] X. Zhao, H. Cao, B.J. Coleman, et al., Adv. Mater. Interfaces 9 (2022) 2200480.
[85] K. Liang, A. Tabassum, A. Majed, et al., InfoMat 3 (2021) 1422–1430.
[86] T. Zhang, L. Chang, X. Xiao, Small Meth. 7 (2023) 2201530.
[87] T. Hu, Z. Li, M. Hu, et al., J. Phys. Chem. C 121 (2017) 19254–19261.
[88] T. Hu, J. Wang, H. Zhang, et al., Phys. Chem. Chem. Phys. 17 (2015) 9997–10003.
[89] G. Gao, A.P. O'Mullane, A. Du, ACS Catal. 7 (2016) 494–500.
[90] R. Thakur, A. Vahid Mohammadi, J. Moncada, et al., Nanoscale 11 (2019) 10716–10726.
[91] D. Kim, T.Y. Ko, H. Kim, et al., ACS Nano 13 (2019) 13818–13828.
[92] A. Olshtrem, S. Chertopalov, O. Guselnikova, et al., 2D Mater. 8 (2021) 045037.
[93] H. Jing, B. Lyu, Y. Tang, et al., Small Sci. 2 (2022) 2200057.
[94] C. Zhou, D. Wang, F. Lagunas, et al., Nat. Chem. 15 (2023) 1722–1729.
[95] J. Hadler-Jacobsen, F.H. Fagerli, H. Kaland, et al., ACS Mater. Lett. 3 (2021) 1369–1376.
[96] Y. Lee, S.J. Kim, Y.-J. Kim, et al., J. Mater. Chem. A 8 (2020) 573–581.
[97] A. Lipatov, M. Alhabeb, M.R. Lukatskaya, et al., Adv. Electron. Mater. 2 (2016) 1600255.
[98] M. Seredych, C.E. Shuck, D. Pinto, et al., Chem. Mater. 31 (2019) 3324–3332.
[99] W. Cui, Z.Y. Hu, R.R. Unocic, et al., Chin. Chem. Lett. 32 (2021) 339–344.
[100] X. Sang, Y. Xie, M.W. Lin, et al., ACS Nano 10 (2016) 9193–9200.
[101] R. Ibragimova, P. Rinke, H.P. Komsa, Chem. Mater. 34 (2022) 2896–2906.
[102] J. Li, R. Qin, L. Yan, et al., Inorg. Chem. 58 (2019) 7285–7294.
[103] A. Al-Temimy, K. Prenger, R. Golnak, et al., ACS Appl. Mater. Interfaces 12 (2020) 15087–15094.
[104] L.N. Shi, L.T. Cui, Y.R. Ji, et al., Coordin. Chem. Rev. 469 (2022) 214668.
[105] V. Natu, M. Sokol, L. Verger, et al., J. Phys. Chem. C 122 (2018) 27745–27753.
[106] C.E. Shuck, M. Han, K. Maleski, et al., ACS Appl. Nano Mater. 2 (2019) 3368–3376.
[107] V. Kotasthane, Z. Tan, J. Yun, et al., ACS Appl. Nano Mater. 6 (2023) 1093–1105.
[108] J. Halim, M.R. Lukatskaya, K.M. Cook, et al., Chem. Mater. 26 (2014) 2374–2381.
[109] Q. Zhang, R. Fan, W. Cheng, et al., Adv. Sci. 9 (2022) 2202748.
[110] M. Shekhirev, J. Busa, C.E. Shuck, et al., ACS Nano 16 (2022) 13695–13703.
[111] X. Li, X. Ma, H. Zhang, et al., Chem. Eng. J. 455 (2023) 140635.
[112] J.L. Hart, K. Hantanasirisakul, A.C. Lang, et al., Nat. Commun. 10 (2019) 522.
[113] W.Y. Chen, X. Jiang, S.N. Lai, et al., Nat. Commun. 11 (2020) 1302.
[114] J. Choi, M.S. Oh, A. Cho, et al., ACS Nano 17 (2023) 10898–10905.
[115] J. Ji, L. Zhao, Y. Shen, et al., FlatChem 17 (2019) 100128.
[116] G.S. Lee, T. Yun, H. Kim, et al., ACS Nano 14 (2020) 11722–11732.
[117] X. Zhao, A. Vashisth, E. Prehn, et al., Matter 1 (2019) 513–526.
[118] Y. Chae, S.J. Kim, S.-Y. Cho, et al., Nanoscale 11 (2019) 8387–8393.
[119] T. Wu, P.R.C. Kent, Y. Gogotsi, et al., Chem. Mater. 34 (2022) 4975–4982.
[120] X.Y. Wang, S.Y. Liao, H.P. Huang, et al., Small Meth. 7 (2023) 2201694.
[121] L. Liao, D. Jiang, K. Zheng, et al., Adv. Funct. Mater. 31 (2021) 2103960.
[122] K. Li, X. Wang, S. Li, et al., Small 16 (2019) 1906851.
[123] A. Vahid Mohammadi, M. Mojtabavi, N.M. Caffrey, et al., Adv. Mater. 31 (2019) 1806931.
[124] N.M. Caffrey, Nanoscale 10 (2018) 13520–13530.
[125] L. Ding, L. Li, Y. Liu, et al., Nat. Sustain. 3 (2020) 296–302.